Quaternary Geochronology
February 2021, Volume 61, Pages 101115 (19p.)
https://doi.org/10.1016/j.quageo.2020.101115
https://archimer.ifremer.fr/doc/00646/75803/

Quaternary evolution of the Golo river alluvial plain (NE Corsica, France)

Molliex Stéphane [1, 2, *], Jouet Gwenael [3], Blard Pierre-Henri [2, 3], Moreau Jonathan [4, 5], Demartini Julie [6], Storms Joep E.A. [7], Vella Claude [5], Aster Team [5]

[1] Laboratoire Geosciences Océan UMR CNRS 6538, Institut Universitaire Européen de la Mer, Place N. Copernic, 29280, Plouzané, France
[2] CRPG, UMR 7358, CNRS-Université de Lorraine, 15 Rue Notre Dame des Pauvres, 54501, Vandœuvre-lès-Nancy Cedex, France
[3] Laboratoire de Glaciologie, DGES-IGEOS, Université Libre de Bruxelles, 1050, Bruxelles, Belgium
[4] IFREMER, Département Geosciences Marines, Z.I. Pointe Du Diable, BP70, 29280, Plouzané, France
[5] Aix-Marseille University, CNRS-IRD-Collège de France, UM34 CEREGE, BP 80, 13545, Aix-en-Provence Cedex 4, France
[6] ODARC, Avenue Paul Giacobbi, BP 618, 20601, Bastia Cedex, France
[7] Department of Geoscience and Engineering, Delft University of Technology, Delft, the Netherlands

* Corresponding author : Stéphane Molliex, email address : smolliex@gmail.com

Abstract :

The Golo River drains a steep catchment (average gradient of 30 m km−1, surface of 1214 km2) in the northeast part of Corsica Island, delivering sediments to the Ligurian Sea. In this study, we review and revise the geologic map and constrain the extent of the Golo coastal alluvial plain formations and their relative and absolute chronology. To update the surface extent of each formation, we performed a geomorphologic analysis with DEMs and satellite imagery data coupled with an extensive pedogenic and sedimentary field observations database, including a new borehole of 117,4 m depth. Additionally, we performed in-situ cosmogenic 10Be analysis from a depth-profile in the well-preserved alluvial terrace Fy2, yielding a minimum age of 70 ka for its emplacement. Our new chronology, based on cosmogenic 10Be and soil chronosequences, implies older ages than those previously obtained with luminescence methods. Soil mixing by bioturbation is proposed as a possibility to explain differences between luminescence and 10Be ages. In this scenario, 10Be dates the original deposition of the alluvial terrace, while luminescence dates a later soil development. We highlighted at least five outcropping alluvial terraces in the Golo coastal plain, which are controlled by sea-level fluctuations and were most likely deposited during past sea-level highstands (close to present-day sea-level). Moreover, we identified from a borehole more than 117 m of coarse fluvial sediments in the plain, that do not outcrop at the surface. New cosmogenic 26Al/10Be burial ages suggest that this sedimentary unit results from a thick accumulation of fluvial material filling a zone significantly affected by subsidence, probably accommodated by a normal fault during the Early Quaternary.

Keywords : alluvial plain, 10Be depth-profile, Quaternary, Geomorphology, Electric Resistivity Tomography, soil sequence chronology, Corsica, terraces

1- INTRODUCTION

Coastal alluvial plains are key places for understanding sediment storage in a source-to-sink approach (e.g. Sømme et al., 2011; Blum et al., 2013). However, the consequences of aggradation/degradation cycles in coastal plains due to Quaternary sea-level oscillations make stratigraphic correlations difficult, with upstream (alluvial terraces) or downstream (shelf sediment accumulation) deposits. Since a decade, alluvial plains focused new research efforts, thanks to the development of relevant tools, such as dating methods on fluvial sequences. Moreover, these settings record paleo-environmental parameters controlling sediment fluxes, such as tectonics,

climate or sea-level fluctuations (e.g. Twidale, 2004; Allen, 2008). In many cases, the extent of alluvial depositional terraces in alluvial plains is mainly based on topographic constraints, such as breaks in slope and escarpments (e.g. Conchon, 1975). Mapping the accurate lateral extension of alluvial terraces and determining their in-depth geometry remain often problematic and suffer from large uncertainties. Notably, the relevant resolution of topographic data is not always available and geophysical surveys are sometimes difficult to conduct in anthropogenic areas.

The geochemical maturity of an alluvial soil increases with age: while Holocene deposits are not weathered, soils from Pleistocene alluvial deposits of Mediterranean periglacial areas are matured, rich in clay, and may become reddish after experiencing several warm phases of Quaternary climatic cycles (e.g. Baize and Girard, 2008; Legros, 2012). Studying chronology of soil sequences on alluvial terraces in addition to geomorphic analysis is thus a very efficient way to determine relative chronology of deposits (Hubschman, 1973; Bornand, 1978; Delmas et al., 2015). Moreover, the use of terrestrial cosmogenic nuclides has proven its efficiency for absolute dating of alluvial deposits (e.g. Granger et al., 1995; Hancock et al., 1999; Brocard et al., 2003; Siame et al., 2004; Molliex et al., 2013).

The high and steep topography of Corsica leads to a strong sensitivity of sediment transfers due to regional climate changes, even for moderate variations (Kuhlemann et al., 2008a). The Golo River system (Eastern Corsica) is considered as a reactive system (Allen, 2008), characterised by a fast sediment transfer from the catchment to the sink (Sømme et al., 2011; Calvès et al., 2013; Forzoni et al., 2015), and rapidly reacts to climate changes. Sediment volumes deposited in the alluvial plain and the deep-sea fan during the Holocene are compatible with sedimentary fluxes inferred from cosmogenic denudation rates in the catchment (Sømme et al., 2011; Calvès et al., 2013; Molliex et al., 2017). However, some studies suggest that alluvial terraces in the plain may be diachronous and that the Golo River may have deposited sediment by aggradation along its entire profile at any time during the late Quaternary. Such climatically-driven pulses in sediment supply may hamper detailed stratigraphic correlations (Conchon, 1978; Sømme et al., 2011; Forzoni et al., 2015). The chronology of the Golo alluvial terraces was first established from relative dating: Conchon (1975, 1977) associated each terrace to a full glacial cycle. Later, luminescence methods applied on sand lenses of outcropping terraces (OSL on quartz and IRSL on feldspar) suggested younger ages for Fy1, Fy2, Fy3 terraces, in correlation with smaller climatic oscillations (Somme et al., 2011; Skyles, 2013; Forzoni et al., 2015) (Table 1). Moreover, luminescence dating yields ages of terrace aggradation that are not always internally consistent, and do not always correspond to climatic oscillations and full glacial stages. Sediment buffering in the alluvial and coastal plain may play an important role in the transfer from the source to the sink and may alter a simple relationship between climate and deposition in the alluvial plain (Somme et al., 2011; Calves et al., 2013). Obtain new absolute ages from the sedimentary material of the Golo alluvial plain is thus key to progress on understanding these processes.

In this paper, we present an updated geological model of the Golo alluvial plain based on new data acquired both in surface (geomorphology, pedology) and depth (borehole, Electrical Resistivity Tomography). We also revised the chronology of formations using new cosmogenic nuclides data (^{10}Be depth profile and ^{26}Al/^{10}Be burial ages). Finally, we discuss the Quaternary evolution of the Golo coastal alluvial plain in response to Quaternary climate and tectonic forcings.

2- GEOLOGICAL SETTING

Corsica is an island of 8,722 km^2 located in the northern part of the western Mediterranean, in the Ligurian Sea. It is characterized by a steep mountainous morphology, with elevations reaching more than 2,700 m (Fig. 1A).

With a catchment area of 1,214 km² and a length of 89 km, the Golo is the largest river in Corsica (Fig. 1A). Originating from 1,991 m, the Golo flows mainly eastward up to the Ligurian Sea with an average gradient of 30 m km^{-1} (Fig.1A). There are almost no preserved alluvial terraces in the upper part of the catchment, due to the very steep and confined nature of the valleys. Despite the relatively steep slopes, there is no evidence of active or paleo-landslides; all colluvial fans being covered by dense vegetation (Sømme et al., 2011). Its main tributaries are the Asco (34.1 km; 165 km²), Tartagine (30.2 km; 136 km²), Casaluna (25.3 km; 100 km²), and Lagani rivers (22.1 km; 47 km²) (Molliex et al., 2017) (Fig.1). The Golo catchment drains two main structural domains: upstream, the magmatic Hercynian domain constituted by Paleozoic crystalline rocks (granite, rhyolites, gneiss) and, downstream, the metamorphic Alpine domain composed of ophiolites and low-gradient metamorphic Mesozoic sediments (mainly phyllites), respectively (Fig.1B).

Corsica is characterised by a complex tectonic history (Mattauer et al., 1981; Harris, 1985; Fournier et al., 1991; Loÿe-Pilot et al., 2004; Fellin et al., 2006; Danisik et al., 2007). Exhumation of the inner part of the island due to tectonic motions mainly occurred in the Miocene (Fellin et al., 2005a; Kuhlemann et al., 2008b). Since the late Miocene, no major tectonic events have affected Corsica. However, transpressive faulting within the late Miocene to Quaternary units suggest that far-field compressional stresses still affect northeastern Corsica to the present-day (Fellin et al., 2005b; Serrano et al., 2013). These stresses could probably be responsible for a Plio-Quaternary tilting of the alluvial plain, the adjacent coastal and shallow marine deposit (Conchon, 1975, 1978, 1999; Kuhlemann et al., 2008b; Serrano et al., 2013).

Corsica is experiencing a subtropical Mediterranean climate with strong seasonal variability. The mean annual temperature averaged over the 1981-2010 period is 15.9°C in the Golo alluvial plain (weather station of Bastia, Poretta airport, 10 m above sea level, id: 20148001; (Meteo-France database; https://donneespubliques.meteofrance.fr/?fond=produit&id_produit=117&id_rubrique=39)). Mean monthly temperature varies between 9°C in January and 24.4°C in August. Mean precipitation is spatially variable, ranging from 700 mm yr^{-1} in the Golo alluvial plain (sea level) to 1300-1400 mm.yr^{-1} in the highest parts of the Golo catchment (~ 2,000 m) (Kuhlemann et al., 2008b; Sømme et al., 2011). Strong seasonal variations in precipitation result in high variability of the river discharge: while the mean annual value is 14.8 m^3.s^{-1}, the peak of discharge may reach 734 m^3.s^{-1} (HYDRO French Database, www.hydro.eaufrance.fr; Valpajola station 1969-2019). Vegetation is dominated by evergreen bushes and trees in the lowlands, with increasing amounts of deciduous and pine forest at higher altitudes (Reille et al., 1997; 1999). There is no permanent ice present in the present-day catchment area, but the uppermost part of the Golo watershed was glaciated during the Last Glacial Maximum (LGM) (23-19 ka ; Mix et al., 2001) and subsequent glacial phases (Kuhlemann et al., 2005; Krumrei, 2009). During the LGM, the Equilibrium-Line Altitude (ELA) varied from 1,400 to 2,000 m in the catchment, and glaciers covered up to 7 % of the catchment area (Kuhlemann et al., 2005).

During glacial stages, Corsica was characterised by cold and dry conditions, with mean annual temperature about 9 °C cooler than present (Kuhlemann et al., 2005; Kuhlemann et al., 2008a; Krumrei, 2009), a 20-30% decrease of mean annual precipitation (Peyron et al., 1998; Allen, 2008), even if some authors argue for a possible increase in precipitation during the LGM (Kuhlemann et al., 2008a), and a herbaceous and steppe vegetation.

The chronology of the Late Quaternary glacier development, based on lateral moraines extent (Conchon, 1975, 1986), has recently been updated by cosmogenic nuclide surface exposure dating (Kuhlemann et al., 2005; Kuhlemann et al., 2008a; Krumrei, 2009).

Alluvial terraces of the Golo River are mainly preserved as depositional terraces in the lowland plain, between 0 and 100 m above present-day sea-level. This plain is only 11 km wide and consists of sediments from three alluvial systems. Golo terraces constitute the main part of the alluvial plain, but alluvial deposits from two smaller coastal catchments, the Bevinco to the North and Fium Alto to the South (Fig.1A) are also present. In the upper part of the plain, Golo-derived alluvial deposits are sometimes mixed with locally sourced colluvial fan deposits. Alluvial deposits consist of poorly-sorted, well-rounded pebbles, cobbles, and boulders supported by a clayey to sandy matrix. Occasionally, well-sorted sand lenses can be found. They have been interpreted as fluvial braided channel deposits (Somme et al., 2011; Forzoni et al., 2015). Bevinco and Fium Alto Rivers deposits are easily distinguishable on the field, since they are exclusively constituted by Alpine domain-originated pebbles. The relative age of Golo terraces have been historically based on the weathering intensity of clasts (e.g. Conchon, 1975, 1978). Indeed, clasts display a large range of weathering, from surface oxidation to the full destruction of the clasts internal integrity (e.g. plutonic rocks such as granite, gabbro). Secondary clay content as a residual product of chemical weathering has also been used for classifying and dating alluvial terraces of Golo. The characteristics of each deposit (called Fz for the most recent to Fv for the oldest) of the Golo alluvial plain are synthetized in Table 1 (Conchon, 1975, 1978). Their relative age is currently based on correlations of moraines and weathering profiles (Conchon, 1975, 1978).

3- METHODS AND DATA

3-1 Geomorphology

Since the resolution of available Digital Elevation Model (DEM) in the Golo alluvial plain was not sufficient, we compiled a DEM from the digitized 1/25000-scale topographic map from the French Geographic institute (IGN), complemented by a microtopographic differential GPS survey in areas of interest (e.g. alluvial terraces boundaries, local depression or bulges). From this DEM, we compute gradient slope map and we extracted the theoretical hydrologic network using ArcGis software®. In addition, satellite images (BD Ortho® from IGN and PLEIADES® from the French spatial studies institute CNES), as well as field observations, were used to map surface characteristics such as vegetation cover, density, degree of development of hydrologic network or flooding area. Longitudinal and transversal topographic cross-sections are also performed and linked with surface soil data.

3-2 Soil chronosequence

Complete evolution of a soil overlaps several 100 ka-climatic cycles. In a sequence of Quaternary alluvial deposits, different levels of soil evolution can be evidenced (Vreeken, 1975). A chronosequence of soils can thus be interpreted as resulting from deposition/alteration cycles leading to the setting of successive terraces. Soils are open systems that experience non-homogenous processes such as denudation and pedogenesis that may lead to differences in soil formation characteristics (Durand et al., 2007). However, low-gradient alluvial plains such as the Golo coastal plain undergo limited denudation (Molliex et al., 2013; Delmas et al., 2015) and are thus suitable landforms for estimating soil formation rates and for assigning relative ages of alluvial deposits.

An extensive soil study was performed by the "Corsica's agricultural and rural development office" (ODARC) (Demartini and Favreau, 2011), with 1951 auger drillings up to 1.2 m depth. The high sample density (> 23 samples/km²) ensures an accurate representation of soil distribution in both alluvial plain and coastal zone. The collected data include soil colour, type of material, texture or presence of leached horizons, in agreement with the French updated pedologic repository (Baize and Girard, 2008) and correlated with the international Food and Agricultural Organization world reference base for soil resources (FAO, 2014). Based on this extensive database, we defined a classification based on petrology and clast content, texture and hydromorphic behaviour, degree of weathering of parental material and different levels of soil evolution. This classification can be used as an independent relative time control assuming that there is a tight relationship between the soil evolution and its age (Conchon, 1975, 1978, 1980).

3-3 Electrical Resistivity Tomography

Electrical Resistivity Tomography (ERT) allows for imaging the electrical properties of the ground layers (resistivity / conductivity). Contrasts in resistivity could be interpreted as facies differences (grain-size, clay content and water content). This method is efficient to characterise alluvial deposits (Gourry et al., 2003; Crook et al., 2008). Here, we used a 64 stainless electrodes Schlumberger protocol for ERT profile acquisition. We sometimes elongate the profile by using rollover acquisitions (see Loke and Barker, 1996 for more details). The distance between electrodes is 10 m and allows an interpretation up to a 90 m depth. In order to obtain true value of depth and resistivity, we used RES2DInv software (Loke and Barker, 1996) for data inversion. The inversion algorithm is based on a smoothness constrained least-squares approach (Sasaki, 1992). The Root Mean Square (RMS) error gives a measure of the difference between measured and inverted models. Interpretations of ERT profiles rely on a calibration realized from field observations and the local borehole database provided by the "Banque de données du sous-sol" (BSS) of the French Geological Institut BRGM (http://infoterre.brgm.fr).

A survey of 53 ERT profiles has been performed in the plain, for a total of 38.5 km-length. Only two representative profiles are presented in this paper. The first one is a 630 m-long East-trending ERT profile performed close to Casamozza, about 80 m eastward from the basement foothills. It permitted to characterize thicknesses of different alluvial deposits, which all crop out along the profile. The second one is a 950 m long N-trending ERT profile aiming to constrain terraces thicknesses and geometry on both sides of the Golo River.

3-4 Borehole GBEC5-2

In order to improve the ground-truth stratigraphy of the Quaternary nested terraces of the alluvial plain and their relationship with the bedrock, a 117.4 m-depth core borehole (GBEC 5-2) was drilled by in December 2012 by the Fugro Company, using a cable drill with a diamonds crown. GBEC5-2 is located transversally to the present-day Golo River, about 2 km eastward of the upper limit of the plain (9.45532°E; 42.52767°N; 18 m; WGS84). The cores were first described on the field, then detailed observations were obtained in the laboratory. The recovery rate is about 80% and is better at larger depths of the drilling. In order to identify differences in stacked alluvial deposits, we performed a detailed petrographic study of the pebbles of the drilled material, following the pioneer work of Conchon (1975; 1978) (Table 1). In practice, we identified all pebbles coarser than 4 cm and classified them into 6 types of rocks, representative of the two main structural units of the Golo catchment. We identified 3 types of rocks for the Hercynian crystalline domain: Permian volcanism rocks (mainly rhyolites),

granitoids, and metamorphic basement rocks (mainly gneiss). For the Alpine domain, we defined the 3 categories: phyllites, ophiolites and sedimentary rocks. A seventh marginal class is composed of rocks that do not belong to the six main categories. A total of 1,252 pebbles have been identified (about 11 pebbles per meter of core). To avoid random sampling bias and recuperation issues, we smoothed the results by analysing intervals of 2 m and applying a running average over 3 intervals (6 m).

3-5 ^{10}Be - ^{26}Al cosmogenic nuclide dating

In situ cosmogenic nuclides represent powerful tools to estimate the duration of a soil exposure to cosmic rays at the Earth's surface (e.g. Gosse and Phillips, 2001; Dunai, 2010). Exposure durations of alluvial layers exposed to denudation can be determined by the measurement of *in-situ*-produced ^{10}Be concentrations along depth profiles (e.g. Siame et al., 2004; Braucher et al., 2009; Hidy et al., 2010; Molliex et al., 2013, Saint-Carlier et al., 2016). The obtained age corresponds to the end of terrace aggradation. In comparison to single dating from surface samples, vertical profiles offer the opportunity to estimate both the exposure duration and the denudation rate, which leads to more accurate ages (Braucher et al., 2009). The CICO profile is in the Fy2 alluvial terrace, at an elevation of 5 m, far from the natural edge of the terrace. It was sampled along a recent excavation of an exploited gravel pit. Eleven samples of single white quartzite or granite clasts were collected along this 4.9 m-vertical section. All selected cobbles are approximately of the same size (~20 cm). For surface sample, the human-made scouring of terrace surface for the gravel pit exploitation leads us to sample not directly on the profile but in the nearby ground. Eight white quartzite pebbles from this surface were amalgamated and analysed for ^{10}Be. Depths of all samples in the profile were measured and corrected for the non-vertical orientation of the human-made scouring. We also applied $^{26}Al/^{10}Be$ burial dating on two samples from the GBEC5-2 borehole, at 37.8 m (B5S59) and 116.5 m (B5S144), respectively. For these two samples, sands (250-1000 µm) from the matrix have been extracted by leaching about 10 cm of a half-core.

Chemical treatments of samples were carried out at the "Laboratoire National des Nucléides Cosmogéniques" (LN2C) at the "Centre Européen de Recherche et d'Enseignement des Géosciences de l'Environnement" (CEREGE, Aix-en-Provence, France) and at PRIME lab (Purdue University, USA). First, samples were crushed into a 250-1000 µm fraction. Then, they were sieved and leached several times in a mixture of HCl and H_2SiF_6, up to the dissolution of all mineral fractions, except quartz. Atmospheric ^{10}Be was removed from quartz grains by 3-times 40% HF successive leaching, aiming at the dissolution of 10% of quartz at each step. The cleaned quartz minerals were then completely dissolved in hydrofluoric acid after addition of 100 µl of an in-house 3.10^{-3} g/g ^{9}Be carrier solution prepared from deep-mined phenakite (Merchel et al., 2008). Hydrofluoric and perchloric fuming removed fluorides. Then, cation and anion exchange chromatography permitted to eliminate iron, manganese, and other elements and obtain pure beryllium and aluminium oxides. Beryllium and Aluminium oxides were mixed to a 325-mesh niobium powder prior to measurements of the $^{10}Be/^{9}Be$ by accelerator mass spectrometry (AMS). For the samples of the terrace profile, $^{10}Be/^{9}Be$ ratios were measured with the "Accélérateur pour les Sciences de la Terre, Environnement, Risques" (AMS-ASTER) national facility. For the borehole samples, $^{10}Be/^{9}Be$ ratios were measured both at the AMS-ASTER and at the "Purdue Rare Isotope Measurement Laboratory (AMS-PRIME). All $^{26}Al/^{27}Al$ ratios were measured at PRIME lab (Purdue University), as well as the ^{27}Al concentrations. The measured ratios were normalized using the KNSTD07 standardization for $^{10}Be/^{9}Be$ (Nishiizumi et al., 2007) and KNSTD standardization for $^{26}Al/^{27}Al$

(Nishiizumi, 2004). AMS internal counting statistics, chemical blank measurements and AMS internal error (0.5%) have been taken into account to correct for analytical uncertainties (Arnold et al., 2010). To obtain the most probable exposure denudation solutions for CICO profile, we used the ^{10}Be profile best-fit model of Saint-Carlier et al. (2016). This Matlab© code is derived from the Hidy et al. (2010) Monte Carlo model and considers the stochastic variability of the inherited component, which is the ^{10}Be concentration of the detrital material before their deposition. In the modeling, we used the world averaged SLHL spallation production rate of 4.13 ± 0.20 at.g^{-1}.yr^{-1} computed with the CREp calculator (https://crep.otelo.univ-lorraine.fr/#/, Martin et al., 2017), with the Lal/Stone time dependent scaling (Stone, 2000; Balco et al., 2008), the ERA40 atmosphere (Uppala et al., 2005) and the geomagnetic reconstruction of Muscheler et al., (2005). The contribution of muons to the production rate was calculated using the parameters of (Braucher et al., 2011). The average density of the alluvial deposit, measured from the GBEC5-2 borehole, is 2.2±0.2 g.cm^{-3}. We used the Chi-2 method to define the best exposure-denudation solutions permitting to fit the data (Siame et al., 2004 ; Molliex et al. 2013; Saint-Carlier et al., 2016) and the (Chi-2+1) domain constrains the uncertainty (Granger et al., 1996).

^{26}Al/^{10}Be burial ages were computed assuming that, before transport and burial, the detrital material was submitted to steady state denudation (e.g. Granger et al., 1996). This assumption is realistic considering the fast sediment transfer due to the steep Golo River catchment morphology and the slow present-day denudation rates (~0.05 mm ka^{-1}) (Molliex et al., 2017). Then, it is supposed that burial was rapid enough to ensure a complete and definitive shielding. The Matlab© code and the parameters summarized in (Blard et al. 2019a,b) were used to compute the ^{26}Al/^{10}Be burial ages. This approach considers that the altitude of pre-burial exposure is the mean elevation of the Golo watershed, 926 m.

4- RESULTS

4-1 Geomorphology

The alluvial plain is a fairly flat eastward dipping surface characterized by a mean elevation of 36 m asl (above sea level) and reaching locally 127 m asl (Fig. 2). The elevation rapidly decreases eastward (from 127 m asl to 15 m asl; brown to yellow in Fig. 2) from the Alpine foothills to the middle of the plain and then moderately decreases from the middle of the plain to the shoreline (from 15 to 0 m asl; yellow to green in Fig. 2). Three geomorphological domains in the Golo alluvial plain can be individualized from elevation and slope repartition. They are highlighted by different grey tones on three longitudinal and three transversal topographic sections (Fig. 3A and 3B, location of profiles in Fig. 2). From the West to the East, it corresponds respectively to the Upper, Middle and Lower Plain (Fig. 3). These compartments are locally separated by main slope breaks. We defined the Upper Plain considering slopes higher than ~ 1°. They locally reach 2.7° in the northernmost part. The minimum elevation is 15 m. The Middle Plain slopes range between 0.7° and 0.2° and elevation between 3 and 34 m (Fig. 3A and 3C). Lower Plain slope is always lower than 0.1° and its maximal elevation is 15 m (Fig. 3A and 3C). The eastward slope gradients are also imprinted by incision of the modern Golo River valley as shown by transversal profiles in each morphological domain (Fig. 3B). In the Upper Plain, the Golo Valley is 130 m wide and 5 m deep (Fig. 3B profile E). In the Middle Plain, the two flanks of the main Golo's channel gradually disappear seaward (Fig. 3B profile F). In the Lower plain, the valley is not anymore incised (Fig. 3B, profile G).

Morphologically, the Upper Plain is also characterized by dendritic stream channels where second-order streams are widely developed, while the Middle plain is predominantly characterized by single channel streams and a sparse hydrologic network. Second-order streams are badly developed in the Lower plain. Upper and Middle plain are mostly covered by oak vegetation, anthropogenic constructions or cultivated fields, while Lower Plain vegetation is constituted by a mix of aquatic and shrubs swamp vegetation. Lower Plain may be flooded during extreme Golo flood events. Several coastal features can also be recognised in the Lower Plain such as sandy dunes and a prograding beach ridge complex with a width varying between 380 and 950 m.

4-2 Geological mapping and soil chronosequence

The type of soils in the Golo alluvial plain depends on i) the composition of pebbles in the alluvial sheets on which they are developed; (ii) their degree of maturation, that depends on time. This degree of maturation can thus be an efficient criterion for relative dating of alluvial terraces. We followed the nomenclature used in the previous map published by the French Geological Survey Office (Lahondère et al., 1994). A synthesis of the criteria used to classify terraces in function of their soil specificities is presented in Fig. 4. We summarized below and in the Fig. 4 the soil and morphological characteristics of each geological unit, from the youngest to the oldest and compare these characteristics with previously published ages and terrace nomenclature (Table 1). The classification of Golo alluvial plain deposits resulted in the definition of 8 soils, including 6 which could be related to alluvial deposits. Fig. 5 displays the revised geological map of the Golo alluvial plain, based on soil chronosequences and morphological analysis.

Modern deposits are Mz, Fz and Fzl. (i) Mz is the littoral fringe, it is composed of a unit of prograding sandy beach ridges that could extend up to 950 m inland. Soil is not developed, and only sparse vegetation is present on these sandy beach ridges. (ii) Fz represents the present-day alluvial deposits, characterized by a Raw Fluvisol, a term used for the surface of modern active streams deposits (FAO, 2014). The formation is constituted either by gravelly-sandy braidplain deposits and finer grained (sand) palaeo-meanders (mainly to the east) and lies in the active bed of the Golo River (Fig. 5). Pebbles and cobbles are fresh and there is no clue of any soil horizons. (iii) Fzl corresponds to fine-grained (silt) sediments which are interpreted as modern floodplain deposits which overlies older alluvial terraces (Sømme et al., 2011). It is located in the lower plain (Fig. 5). The lateral extent of this unit is associated with considerable uncertainty because it is deduced from a compilation of isolated observations (mechanic soundings, boreholes or field observations during or after flooding events; Demartini and Favreau, 2011).

Fy3 alluvial formations are characterized by the development of Typical Fluvisols, a mix of pebbles and sands in surface, with a beginning of soil formation, with weak horizon differentiation. Pebbles and cobbles are weakly weathered. Sometime a beginning of decarbonation may occur (Fig. 4). Fy3 typically constitutes the flood bed of almost all rivers through the plain.

Fy2 alluvial formations are characterized by the development of Brunisols, characterized by a brownish colour, composed by three horizons and moderately developed in depth (about 20 cm). Granite and phyllites elements are weathered and contribute to the development of a thin brown clay-rich horizon. These soils are leached, but not heavily, a differential weathering that led to the formation of Al and Fe oxides, responsible for the overall brown colour (Fig. 5). Fy2 is mostly located to the North of the present-day Golo River (98 %). It extends from the basement foothills to the middle plain (Fig. 5) and present an average slope of ~0.2° toward the sea (Fig. 3).

Fy1 alluvial formations are characterized by the development of Reddish Brunisols, characterized by a well-developed leached surface horizon, a thickness comprised between 10 and 50 cm and yellow to red colours (Fig. 4). They are mainly preserved in the middle (61.5 %) and the upper plain (30.5 %). Fy1 present a mean slope ranging from ~0.3° to the South to ~0.7° to the North (Fig. 3). Fy1 could also be differentiated from Fy2 because of well-developed scarps of several meters between Fy1 (above) and Fy2 (below) (Fig. 5). Based on the arguments discussed for Fy2 chronostratigraphy, this sequence should represent older interglacial alluvial sediments.

Fx alluvial formations are characterized by the development of Luvisols characterized by an extensively leached layer in surface that is nearly free of clay and iron-bearing minerals. A layer of mixed clay accumulation lies below, with high concentrations in available ions. Surface leached horizons are more and more developed with soil maturity (up to 5 horizons) and may exceed several meters in the most evolved soils (Fig. 4). These deposits are mainly located in the upper plain (97 %). Field observations (outcrops and soils) suggest that Fx is only related to minor rivers in the plain (Pietre Turchine, Rasignani, Fig. 5), outside of the Golo catchment area, since it is constituted only by Alpine domain-derived sediment. We did not observe Fx surface deposits that originated from the Golo Catchment, in contrast to previous interpretations (Conchon, 1975, 1978).

Fw is presumably the oldest formation that crops out in the plain. It is characterized by the development of Ferralsols with diffuse horizon boundaries, a clay- and iron oxides- rich horizon mainly composed of kaolinite that can reach a thickness of 1m (Fig. 4). All pebbles and cobbles are affected by such weathering that some of them are entirely destroyed. Some resistant pebbles and cobbles (rhyolite) present a 3-4 cm ring of weathering. Primary clay derived from degradation of clasts feeds into the deeper clay-rich horizon. Fw lies almost exclusively in the upper Plain. Only a small area located to the South of the present-day Golo River presents a combined Hercynian-Alpine provenance clasts assemblage, which is the signature of a Golo River provenance (Fig. 5). The high slope gradient of the Fw surface (> 1°) results in a truncated soil profile with absence of leached horizons. The downstream limit of the Fw terrace is almost always marked by abrupt slope changes from higher to lower slope values (Figs. 2, 3 and 5).

4-3 Electrical Resistivity Tomography

A 630 m-long East-trending ERT profile was performed close to Casamozza. From the results and the mapping of the terraces, three electrical units corresponding to Fy3, Fy2 and Fy1 terraces can be distinguished in the 630 m-long East-trending ERT profile, about 80 m eastward from the basement foothills (Fig. 6A, location in Fig. 5). These units present relative resistivities which slightly decrease with age, with values of 400-800 ohms.m^{-1}, 300-600 ohms.m^{-1} and 240-500 ohms.m^{-1}, for Fy3, Fy2 and Fy1, respectively. Resistivity values for Fw are lower westward, ranging from 80 to 280 ohm.m^{-1}. At depth, resistivity values range from 20 to 80 ohms.m^{-1}, and likely represent a formation that does not crop out at the surface (see part 5.2 for discussion). The mean thicknesses of Fy3, Fy2, Fy1 are 10 to 15 m while mean thickness of Fw is more likely to be 20 m (Fig. 6A). Note that resistivity values are locally scattered due to terrace heterogeneities and/or differences in the conductivity of the groundwater.

Relative resistivity values for Fz, Fy3, and Fy2 terraces in the N-trending ERT profile (Fig. 6B, location in Fig. 5) are about 120-250 ohms.m^{-1}, 300-800 ohms.m^{-1} and 700-800 ohms.m^{-1}, respectively (Fig. 6B).The differences of resistivity between the two profiles may be explained by soil water content and/or the heterogeneity of alluvial

material in relation with the main Golo riverbed distance. A staircase contact is evidenced between Fy3 and Fy2, consistent with a topographic escarpment of approximately 5 m between the two units (Fig. 3; Fig.6B). A similar contact is presumed between the less resistive Fz terrace and the Fy3 terrace. The topographic bulges on both sides of the Golo River consist of human-made dams. The Fy2, Fy3 and Fz alluvial terraces overlie a heterogeneous succession with two stacked layers, a 180-500 ohms.m^{-1} unit, which overlies a 10-80 ohms.m^{-1} unit. Accordingly to GBEC5-2 borehole and field data (cf. Part 4.4), the 180-500 ohms.m^{-1} unit may correspond to Fw terrace, while the 10-80 ohms.m^{-1} unit corresponds to an alluvial sheet not known from the surface (see part 5.2 for discussion). The high resistivity anomaly observed around 90 m depth (Fig. 6B) is possibly an artefact or a local heterogeneity or change in water chemistry, since no change in facies was noticed in the borehole GBEC5-2, that was drilled after the ERT profile (Fig. 7).

4-4 Borehole data

The GBEC5-2 borehole shows a very homogenous 117.4 m of continental alluvial sand and gravel deposits in a clay-dominated matrix (Fig. 7). Marine strata were not deposited and/or preserved in the stratigraphic column. The bedrock was not reached. Conchon (1975, 1977) had already suggested a thick (at least 150 m) stacked braided alluvial sequence underneath the Golo alluvial plain, based on geophysical data (vertical electrical sounding).

There is no sharp transitions in the recovered cores, except within the first 20 m, where two paleosoils are identified by a reddish coloration of the matrix and a complete disaggregation of the clasts. These two reddish levels are at 8.5 and 18.5 m depth, respectively (Fig. 7A). By analogy with the correlation previously made between alluvial formation and their soil evolution, these levels can be interpreted as paleosoils of terraces older than Fy2. Terrace mapping and ERT data suggest that the surface is constituted by Fy3 terrace directly lying on Fy1; Fy2 has been entirely removed by Fy3 erosion. The first reddish level can thus correspond to the top of Fy1 terrace at 8.5 m. In the Golo alluvial plain, Fx is not recognized at surface and Fy1 is often in direct contact with Fw. The second reddish level could thus be interpreted as the limit between Fw and Fy1, at 18.5 m depth (Fig. 7A). The top of an aquifer layer was crossed at 39.5 m depth during drilling (Fig. 7A). It could correspond to a transition between a permeable (above) and an impermeable (below) layer, even if no clear facies change is noticed. Petrologic analyses do not allow for an accurate differentiation of terraces in function of clast petrography. However, it is possible to note that, at about 40 m, pebbles are more weathered, with a drastic decrease of the recovery of pebbles (Fig. 7B). Moreover, granitoids and phyllites are less abundant than rhyolites and ophiolites, which are the more resistant rocks in the catchment (Molliex et al., 2017). If the presence of water may increase the weathering, other causes also have to be considered. Indeed, why water could circulate here and nowhere else? We thus suggest that, at 40 m, this weathered level results in the presence of a paleo-aquifer. This weathered level was probably exposed sufficiently long enough at the surface for removing a large part of soft rocks by erosion. From this depth, composition of pebbles progressively evolved, up to about 60 m depth. Indeed, in the first ~40 m, pebbles from the Hercynian domain represent about 55 % of the total pebbles, and Alpine phyllites pebbles about 10 %. Below 60 m, the content of Alpine phyllites pebbles is much higher (30 % of total pebbles), while Hercynian domain pebbles are represented less frequently (only 40 % of the total pebbles). The zone between 40 m and 60 m depth can be considered as a transition zone between the two

petrologic compositions. No paleosoils nor evidence of any other transition can be identified over the 60-117.4 m core section (Fig. 7A).

4-5 Cosmogenic ^{10}Be and ^{26}Al data

^{10}Be concentrations measured in the CICO vertical depth profile (Fy2 terrace) are compatible with a near exponential decrease with depth (Fig. 8B and Table 2). This indicates that: i) the analysed samples remained in their relative and sampled positions since the terrace deposition and, therefore, that the build-up of in-situ cosmogenic ^{10}Be in this sedimentary material most probably occurred after one single deposition event, ii) the dispersion due to variable pre-exposure is not significant compared to the age of the terrace exposure. The higher concentrations in CICO 70 and CICO 200 samples probably result from a complex pre-deposition exposure history in the upper catchment. The inverse modeling of this profile did not permit to define only one single "denudation - exposure duration" scenario, indicating that the terrace reached what is called steady-state denudation. In this case, the production of ^{10}Be is balanced by the loss due to the surface denudation (Fig. 8). Such configuration only permits to derive a minimum exposure age, a denudation rate and the value of the pre-deposition concentration. The obtained best-fit scenario indicates with a high level of confidence that: i) the exposure duration of terrace Fy2 is at least 70 ka, ii) the surface denudation rate of Fy2 is 10 ± 2 mm.ka^{-1} and iii) the mean inherited ^{10}Be of the Fy2 silico-clastic material is 6×10^4 at.g $(SiO_2)^{-1}$ (Fig. 8B). This value can also be used to calculate a paleo-denudation rate at the time of terrace deposition: 95 ± 4 mm.ka^{-1}.

The $^{26}Al/^{10}Be$ burial ages from the GBEC5-2 borehole are 2.45 ± 0.73 Ma at 37.8 m (sample B5S59) and 2.74 ± 0.95 Ma at 116.5 m (sample B5S144), respectively (Table 3).

5- DISCUSSION

5-1 Chronology of Late Pleistocene events

Aggradation of sediment in alluvial systems depends of slope, base level and sediment transport rate (e.g. Blum and Törnqvist, 2000). In a coastal alluvial plain such as the Golo, fluvial aggradation is strongly controlled by sea-level fluctuations. Fluvial aggradation generally occurs during sea-level highstands, i.e. deglacial (valley filling) and interglacial (upstream overflow) stages (e.g. Blum and Törnqvist, 2000), because fluvial slope may decrease, as well as the transport capacity of sediments. Lowstand alluvial units were deposited on the middle and outer shelf (Sweet et al., 2020). Nevertheless, aggradation in the plain may also occur during glacial stages if sediment supply overloads the channel transport capacity (e.g. Blum and Törnqvist, 2000; Forzoni et al., 2015). In Mediterranean regions, sapropel events are recognized as markers of an increase of freshwater runoff during interglacial stages (Rohling et al., 1991; 2015; Milner et al., 2012, Toucanne et al., 2015) and suggest that sediment supply during glacial and interglacial periods are not very different in average, despite glacial periods are generally recognized to trigger larger input (Kettner and Syvitsky, 2009). Numerical modeling however suggests that the sediment supply during MIS4 and MIS2 was twice the one of the Holocene (Forzoni et al., 2015). In our following interpretations, we therefore consider that aggradation of alluvial material in the present-day emerged Golo coastal plain occurred during sea-level rise, i.e. from deglacial to interglacial stages. This interpretation is supported by the luminescence and ^{14}C dating of the most recent unit (Fy3) of the Golo plain (Sømme et al., 2011; Forzoni et al., 2015) and also by the presence of a past sea-level highstand beach sand level into the terrace Fy1 in the Sagone Gulf (SW Corsica) (Conchon, 1989).

Based on the new cosmogenic ^{10}Be CICO profile dating of Fy2 and relative pedologic observations, we revisit the chronology of the Golo alluvial plain deposits. Old and new chronologies are summarized in Table 1. After the end of the Last Glacial Maximum, during the deglaciation (i.e. ~10-15 ka), Fy3 alluvial sheet was deposited in response to sea-level rise and the increased discharge of sediment supply triggered by glaciers melting in the upper catchment, as demonstrated by hydro-sedimentary simulations (Forzoni et al., 2015), that filled the incised hydrographic network developed during the MIS2 glacial stage. The sediment supply then decreased during the Holocene, leading to a change in fluvial style, from braided (Fz) to meandering (Fzl) deposits (e.g. Blum and Törnqvist, 2000). Fzl deposits are dated by OSL at 3.18 ± 0.98 ka (Skyles, 2013).

Forzoni et al. (2015) suggest elevated temperature post-IR IRSL ($pIRIR_{290}$) ages for Fy2 terrace of 43 ± 4 and 46 ± 7 ka (Fig. 5; Table 4). They associated this deposit to the warming at the onset of MIS 3. Our new in situ cosmogenic ^{10}Be profile in the same terrace yields a minimum abandonment age of 70 ka (at least MIS5a), older than these luminescence ages. Even if some studies suggested the possibility of overestimated ages in ^{10}Be concentration depth profile measurements resulting from heterogeneous residual inheritance in pebbles (Le Dortz et al., 2012), the ^{10}Be CICO profile analysed displays a near perfect exponential decrease with depth (Fig. 8B) and our modelling approach takes into account the impact of inheritance on the exposure duration (Saint-Carlier et al., 2016). On the contrary, our inverse modelling shows that the ^{10}Be CICO profile mandates a minimum deposition age of 70 ka (at least transition MIS 5 / MIS 4) (Fig. 8B). In > 70 ka offshore Golo deposits, Sweet et al. (2020) also identified quartz OSL luminescence ages younger than the deposition ages based on the δ^{18}O chronology. The fact that luminescence ages for sediment older than 70 ka may be underestimated in some context is still a debated topic that may involve several mechanisms, such as the saturation of the thermal signal in quartz (e.g. Steffen et al., 2009; Lowick and Preusser, 2011; Lowick and Valla, 2018) and the grain size dependence of the signal (e.g. Buylaert et al., 2007; Timar et al., 2010; Fan et al., 2010; Timar-Gabor et al., 2017). Forzoni et al. (2015) were aware of these potential limitations and thus applied IRSL on feldspars, instead of quartz. For IRSL, the anomalous fading in feldspars may also lead to a possible age underestimate (e.g. Wintle, 1973; Auclair et al. 2003; 2007; Kars et al., 2008; Li et al., 2018). Forzoni et al. 2015 applied $pIRIR_{290}$ feldspar dating to overcome problems related to early signal saturation (quartz OSL) and anomalous fading (conventional IRSL feldspar dating) (e.g. Li and Li, 2011; Thiel et al., 2011; Buylaert et al., 2012, Kars et al. 2012). Thus, age disagreement can neither be explained by too early saturation, nor by fading. Another bias could arise from the water content estimation, which may overestimate the environmental dose rates and thus underestimate luminescence ages (e.g. Duller, 1994; Jeong et al., 2007; Carr et al., 2019). Indeed, constraining the exact water content for the entire burial period is not a straightforward task. However, even if the wettest possible scenario is considered for these deposits, IRSL age would only increase by ~10%, i.e. from ~45 ka to ~49 ka, which is not enough to explain the observed age difference. Another cause for the ^{10}Be-luminescence discrepancy could be the use of contrasted grain size: ^{10}Be analyses were performed in pluri-centimetric quartz cobbles, while $pIRIR_{290}$ in sand-sized (200-250 µm) feldspars. The sand fraction is sensitive to biological soil mixing, which can be highly effective in exposing grains at the surface, thus resetting the $pIRIR_{290}$ signal (Reimann et al., 2017). The CICO $pIRIR_{290}$ samples are at about 2 m depth and deep-rooted vegetation reach the sandy layer dated by $pIRIR_{290}$ (Fig. 9A), also implying modifications of fluids circulation into the sand layer. Thus, we could reasonably suggest that the luminescence ages for Fy2 have been rejuvenated

by these hydro-biological processes. If correct, this scenario suggests that ^{10}Be dates the original deposition of the alluvial terrace, while luminescence dates the later soil development.

An interesting and complementary observation lies in the sea level, which was 40-70 m below the present-day level during MIS3 (~25-60 ka) (Spratt and Lisiecki, 2016). At this time, the depocenters were located offshore of the current alluvial plain (Sweet et al., 2020), aggradation in the plain was thus very unlikely or limited, while such conditions were favourable to a soil development on Fy2. Based on the cosmogenic ^{10}Be profile (that yields a minimum terrace exposition of 70 ka), relative pedologic observations and comparisons with alluvial regional deposits, we propose that the emplacement of the Fy2 terrace occurred during one of the highest sea-level of MIS 5 (5a, ~82 ka) (or during 5c, 5e, or a composite of all these MIS 5 high sea-level stages). Then, the abandonment age of Fy2 was probably around 70 ka, just after the MIS 5a-4 cooling. This climatic transition very often led to the abandonment of geomorphological surfaces in coastal environments worldwide (e.g., Pedoja et al., 2011), consistently with the chronology of sea-level fluctuations: MIS 5a was indeed the last sea level highstand before the Holocene (Spratt and Lisiecki, 2016). This interpretation would also be consistent with the presence of a Brunisol developed above Fy2, under the cold and dry conditions of MIS 4 to MIS 2 that are not favorable to Fe oxidation. Moreover, alluvial deposits similar in age and soil facies and under a similar Mediterranean climate are widely preserved in Southern France (Brocard et al., 2003; Siame et al., 2004; Molliex et al., 2013, Delmas et al., 2018).

For Fy1, IRSL analyses on feldspar yield $pIRIR_{290}$ ages of 92 ± 11 ka and 100 ± 12 ka (Forzoni et al., 2015) (Fig. 5, Table 4). At that site, there is no evidence of biological perturbations at the IRSL sample level (~4 m depth) (Fig. 9B). If these $pIRIR_{290}$ ages are representative of the deposition age of Fy1, this terrace would have been deposited during MIS 5c. However, the soil developed on Fy1 is widely oxidized (Reddish Brunisol). Fy1 is the youngest reddish terrace, with a soil that is still partially brown, i.e. has not been entirely oxidized. This likely indicates that this terrace experienced just one warm climatic optimum after its deposition. The youngest interglacial stage able to create reddish soils is the Eemian period, MIS 5e, between 124 and 119 ka (Legros, 2012; Delmas et al., 2015; Hughes and Gibbard, 2018), because it is the warmest and the wettest one. Deposition of Fy1 would thus be not much older than MIS 5. Since terraces in the alluvial plain are deposited during highstands, the deposition of Fy1 may have occurred during the MIS 7 to MIS 6 transition (190 ka; Spratt and Lisiecki, 2016; Hughes and Gibbard, 2018). This age would be consistent with the dating of a regional well-preserved terrace level in southern France (Brocard et al. 2003; Molliex et al., 2013, Delmas et al., 2018). However, an MIS 5c age for Fy1, with a reddish soil development during the MIS 5a cannot be totally excluded.

Fx is not present at the surface of the Golo River alluvial plain. Its deposition could correspond to the MIS 10-MIS 11 transition (about 400 ka), because MIS11 is known as one of the warmest interglacial with a high sea-level (Spratt and Lisiecki, 2016; Hughes and Gibbard, 2018).

Two quartz OSL ages for the Fw terrace are reported by Somme et al (2011). They are 44 ± 3 and 61 ± 4 ka (Fig. 5, Table 4). These ages are clearly too young, the samples most likely suffered from quartz saturation as reported by Forzoni et al (2015) and should therefore not be considered. The characteristics of soils developed on this terrace suggest that it experienced at least the last interglacial period (i.e. MIS 5e; 120 ka) (Pedro, 1968; Demartini and Favreau, 2011; Legros, 2012), like Fy1. No more accurate age constraints are available for Fw. We suggest that Fw was probably deposited during the warm interglacials that occurred between MIS 19 and MIS 23; about 800-1000 ka), since this stage corresponds to the first of the 100-ka climatic cycles since the

middle Pleistocene transition; ~0.9 Ma) and is probably one of the best preserved level for Early Quaternary terraces in Southern France (Colomb et Roux, 1978; Dubar, 1984; Delmas et al., 2018).

At lower depth, samples from the borehole GBEC5-2 yield similar $^{26}Al/^{10}Be$ burial durations of 2.45 ± 0.73 Ma at 37.8 m and 2.74 ± 0.95 Ma at 116.5 m in (Table 3). These data indicate that the unknown thick formation evidenced from ~40 to 117 m in the GBEC5 borehole, that is stratigraphically older than the Fw terrace, likely results from accumulation of sediments during the end of the Pliocene or the beginning of the Quaternary, around 2.6 Ma. Despite large uncertainties, these ages suggest that the accumulation rate of sediments was high during this period, implying a rapid infilling of an accumulation space.

5-2 Geodynamic evolution of the Golo alluvial plain

The presence of more than 117 m of continental Quaternary alluvial deposits evidenced in the GBEC5-2 borehole is enigmatic (Fig. 10A; 10B; 10D). Indeed, during the Quaternary, the climatic oscillations lead to strong sea-level variations (up to 120 m), and thus rapid aggradation/degradation cycles in the alluvial plain, with the onset of alluvial terraces in the plain during the highstands and their destruction by incision and erosion during lowstands. In this context (subsidence and sea-level drops and rises), marine deposits should have been preserved in a borehole crossing a 0-100 m range of elevation below the sea level. The sea-level have oscillated only between 50 and -50 m during the Early Pleistocene (Miller et al., 2005; de Boer et al., 2010; Rohling et al., 2014). The base of the GBEC5-2 borehole (at least from -67 m depth) should thus be constituted by marine deposits, even during lowstands. As there are no marine sediments preserved in the borehole, we can postulate than subsidence occurred in the alluvial plain at least since the Plio-Pleistocene transition, 2.6 Ma. Considering the location of the borehole and the chronology of the deposits, subsidence of the Golo River alluvial plain should be invoked to explain a continental infilling. However, the high slope of the old Quaternary terraces and the cut-and-fill geometry of these terraces only 1-km upstream also argue for a long-term uplift of the upstream part of the catchment, in agreement with post-Miocene exhumation of the inner part of Corsica (Fellin et al., 2005a). Given the short distance between these two domains, a tilting of the margin is unlikely to occur. A control by a fault delimiting the eastern subsiding plain and the western highlands is more plausible. Such fault would have accommodated at least 77 m of vertical motion during the whole Quaternary (Fig. 10C). This fault would correspond to the sharp contact between the bedrock and the Quaternary formations, at the western margin of the Golo alluvial plain. There is only sparse evidence of recent tectonic activity documented in Corsica (e.g. Conchon, 1977, 1999; Fellin et al., 2005a; Serrano et al., 2013). No active structure is referenced yet in Corsica and instrumental and historical seismicity is very low (SISFRANCE database). The estimated subsidence rate should be at least 77 m in ~ 2.6 Ma, i.e. ~ 0.03 mm yr^{-1}, consistent with mean deformation rates of active regional tectonic structures in Southern France (0.02-0.01 mm yr^{-1} after Molliex, 2009). The apparent sedimentation rate at the bottom of the borehole is high (~77 m in 0.4 Ma, ~ 0.2 mm yr^{-1}). A part of this accumulation might be due to the infilling of a paleo-valley. However, given uncertainties on $^{26}Al/^{10}Be$ ages (2.45 ± 0.73 and 2.74 ± 0.95 Ma; Table 3) such rates must be considered with caution.

Because of the absence of marine deposits in the borehole deposits, and without evidence of drastic change in sediment supply, we can postulate that the alluvial plain was already filled by continental sediment before the onset of the large eustatic oscillations (~120 m) after the Mid-Pleistocene transition (0.9 Ma; e.g. Gibbard et al., 2010). The onset of the 100 ka glacial cycles after the Mid-Pleistocene transition have probably

increased exhumation and denudation rates (Champagnac et al., 2007; Valla et al., 2011; Hermann et al., 2013). In the Inner Alps the exhumation and denudation of crystalline rocks was enhanced, as evidenced by an increase of the proportion of crystalline rocks among the sediments deposited in the Inner Alps forelands (Petit et al., 1996; Boenigk and Frechen, 2006; Molliex et al., 2013). In Corsica, the same process can be evocated, because post-Miocene exhumation and Quaternary glaciations of the inner part of Corsica (Fellin et al., 2005a) is concomitant with a higher frequency in Hercynian clasts in alluvial deposits. The change in pebbles composition at the 40 m depth in the borehole supports the hypothesis that the sediments located above this depth started to be accumulated after the Mid-Pleistocene transition.

In summary, the upper 40 m-depth of the borehole GBEC5-2 were likely deposited after the Mid-Pleistocene transition, during the Late Pleistocene and the Holocene, with an accumulation rate of about 40-50 m Ma^{-1}. They are mainly composed of material from the higher Hercynian part of the Corsican reliefs. This observation is consistent with an enhancement of the erosional flux from high elevation areas under the glacial conditions of the Late Pleistocene (100 ka glacial cycles), as also documented in the French Alps (Dubar, 1984; Colomb et Roux, 1978). The deposits below ~60 m-depth are constituted by a higher part of Alpine content and could thus be related to pre-glacial conditions, such as those of the Early Pleistocene. There is no evidence of marine sedimentation between 2.6 and 0.9 Ma, thus Early Pleistocene deposits of the Golo River plain reflect continental conditions for a long time, between their deposition (2-3 Ma) and the onset of the Mid-Pleistocene transition (0.9 Ma; Gibbard et al., 2010). The sediment included between ~40 and 60 m-depth could thus be interpreted as the weathered zone of Early Pleistocene deposits. A tilting of the margin with low subsidence rates in the plain (~ 0.03 mm yr^{-1}) should have occurred at least during the Early Pleistocene and perhaps more recently. It is probably superimposed with the motion of a normal fault located in the upstream alluvial plain. Confirming the existence of this fault could motivate future research.

6- CONCLUSION

For a better understanding of the Quaternary evolution of the Golo River alluvial plain, we obtained data from several approaches, including geomorphology, soil studies, sedimentology, ERT profile and terrestrial cosmogenic nuclides dating (^{10}Be and ^{26}Al). We improved the accuracy and resolution of geological mapping of Quaternary alluvial sheets in the Golo plain and provided new chronological constrains based on soil chronosequence and cosmogenic nuclides. We highlighted at least four alluvial terraces within the Golo coastal plain. Their deposition are related to sea-level variations and occurred during sea-level highstands, while incision of the plain occurred during sea-level lowstands. Based on a new ^{10}Be depth-profile, the abandonment age of terrace Fy2 is at least 70 ka, older than it was previously suggested by luminescence dating (~50 ka). This discrepancy between existing luminescence ages and cosmogenic nuclide-based chronology might be due to a difference in the type (grain size) of analyzed sediment. Finer sandy fraction could reflect a soil bioturbation event (dated at ~50 ka by IRSL) that occurred several thousand years after the terrace deposition (dated before 70 ka by ^{10}Be). More detailed studies are required to check this point. Furthermore, we recognized in the GBEC5-2 borehole a thick amount of alluvial deposits (> 117 m), including an unknown formation which lies below the Quaternary alluvial sheets outcropping in the plain. This continental formation, dated at 2.5-3 Ma by the $^{26}Al/^{10}Be$ burial chronometer, can be interpreted as an infill of an Early Pleistocene accommodation space caused by the subsidence of the area at a rate ~ 0.03 mm yr^{-1}. An unidentified fault is probably delimiting the

eastern subsidence plain and the western highlands. Because of its large thickness and despite its moderate lateral extent, the Golo alluvial plain has to be considered as a potential significant storage area in source-to-sink studies.

AKNOWLEDGEMENTS

This research was financed by IFREMER, the “Agence de l’Eau Rhône-Méditerranée-Corse” and also benefited from a State Grant from the French "Agence Nationale de la Recherche (ANR)" in the Program "Investissements d'Avenir" (ANR-10-LABX-19-01, Labex Mer). It was finalized as part of the EROMED ANR program (ANR-17-CE01-0011). JEAS was funded by ALW-NWO (Dutch Organization for Scientific Research, VIDI grant number 864.09.004). We warmly thank Daniel Hermitte, Jean-Claude Parisot, Phillipe Dussouillez for their assistance with ERT and GPS on field, and Angélique Roubi and Nicolas Freslon who were involved in the field explorations and drilling operation. We also thank Francois Galgani and Gwenaelle Bodéré, respectively from IFREMER and BRGM centers in Corsica; for the on-site logistical support. CICO quarry, Jean-Louis Cipriani, the Lucchiana city and the “Mariana et la basse vallée du Golo” association are thanked for their local assistance on field. Elodie Petit and Ewan Pelleter are thanked for their help in petrography. ^{10}Be measurements at the ASTER AMS national facility (CEREGE, Aix en Provence) is supported by the INSU/CNRS, the ANR through the "Projets thématiques d’excellence" program for the "Equipements d’excellence" ASTER-CEREGE action, and IRD. The French CNRS INSU SYSTER partly financed cosmogenic nuclide concentration measurements. ^{10}Be and ^{26}Al measurement at the PRIME AMS facility was performed by MW Caffee and his team. We also warmly thank N. Akçar, T. Reimann, an anonymous reviewer and editor F. Preusser for their fruitful comments that considerably improved the first version of the manuscript.

REFERENCES

Allen, P.A., 2008. Time scales of tectonic landsapes and their sediment routing systems, in Gallagher, K., Jones, S. J., and Wainwright, J., ed., Landscape Evolution: Denudation, Climate and Tectonics over Different Time and Space Scales. Geological Society of London, Special Publication 276, 7-28.

Arnold, M., Merchel, S., Bourles, D.L., Braucher, R., Benedetti, L., Finkel, R.C., Aumaitre, G., Gottdang, A., Klein, M., 2010. The French accelerator mass spectrometry facility ASTER: Improved performance and developments: Nuclear Instruments & Methods in Physics Research Section B-Beam Interactions with Materials and Atoms 268, 1954-1959.

Auclair, M., Lamothe, M., Huot, S., 2003. Measurement of anomalous fading for feldspar IRSL using SAR. Radiation measurements 37(4-5), 487-492.

Auclair, M., Lamothe, M., Lagroix, F., Banerjee, S.K., 2007. Luminescence investigation of loess and tephra from Halfway House section, Central Alaska. Quaternary Geochronology 2(1-4), 34-38.

Baize, D., Girard, M.C., 2008. Référentiel Pédologique : classification des sols établie en France. Editions Quae, 403 pp.

Balco, G., Stone, J.O., Lifton, N.A., Dunai, T.J., 2008. A complete and easily accessible means of calculating surface exposure ages or erosion rates from ^{10}Be and ^{26}Al measurements. Quat. Geochronol. 3, 174–195.

Blard, P.H., Lupker, M., Rousseau, M., 2019a. Paired-cosmogenic nuclide paleoaltimetry. Earth and Planetary Science Letters 515, 271-282.

Blard, P.H., Lupker, M. Rousseau, M. Tesson, J, 2019b. Two MATLAB programs for computing paleo-elevations and burial ages from paired-cosmogenic nuclides. MethodsX 6, 1547-1556 (https://doi.org/10.1016/j.mex.2019.05.01).

Blum, M.D., Törnqvist, T.E., 2000. Fluvial responses to climate and sea-level change: A review and look forward. Sedimentology 47, 2–48.

Blum, M., Martin, J., Milliken, K., Garvin, M., 2013. Paleovalley systems: Insights from Quaternary analogs and experiments. Earth-Science Rev. 116, 128–169.

Boenigk, W., Frechen, M. 2006. The Pliocene and Quaternary fluvial archives of the Rhine system. Quaternary Science Reviews 25(5-6), 550-574.

Bornand, M., 1978. Altération des matériaux fluvio-glaciaires, genèse et évolution des sols sur terrasses quaternaires dans la moyenne vallée du Rhône. State Thesis, Université du Languedoc. 329 pp.

Braucher, R., Del Castillo, P., Siame, L., Hidy, A.J., Bourles, D.L., 2009. Determination of both exposure time and denudation rate from an in situ-produced Be-10 depth profile: A mathematical proof of uniqueness. Model sensitivity and applications to natural cases. Quaternary Geochronology 4, 56-67.

Braucher, R., Merchel, S., Borgomano, J., Bourles, D.L., 2011. Production of cosmogenic radionuclides at great depth: A multi element approach. Earth and Planetary Science Letters 309, 1-9.

Brocard, G. Y., van der Beek, P. A., Bourlès, D. L., Siame, L.L., Mugnier, J.-L., 2003. Long-term fluvial incision rates and postglacial river relaxation time in the French Western Alps from 10Be dating of alluvial terraces with assessment of inheritance, soil development and wind ablation effects. Earth and Planetary Science Letters 209, 197-214.

Buylaert, J. P., Vandenberghe, D., Murray, A. S., Huot, S., De Corte, F., Van den Haute, P., 2007. Luminescence dating of old (> 70 ka) Chinese loess: a comparison of single-aliquot OSL and IRSL techniques. Quaternary Geochronology 2(1-4), 9-14.

Buylaert, J. P., Jain, M., Murray, A. S., Thomsen, K. J., Thiel, C., Sohbati, R., 2012. A robust feldspar luminescence dating method for Middle and Late P leistocene sediments. Boreas 41(3), 435-451.

Calves, G., Toucanne, S., Jouet, G., Charrier, S., Thereau, E., Etoubleau, J., Marsset, T., Droz, L., Bez, M., Abreu, V., Jorry, S., Mulder, T., Lericolais, G., 2013. Inferring denudation variations from the sediment record; an example of the last glacial cycle record of the Golo Basin and watershed, East Corsica, western Mediterranean sea. Basin Research 25, 197-218.

Carr, A.S., Hay, A.S., Powell, D.M., Livingstone, I., 2019. Testing post-IR IRSL luminescence dating methods in the southwest Mojave Desert, California, USA. Quaternary Geochronology 49, 85-91.

Champagnac, J.D., Molnar, P., Anderson, R.S., Sue, C., Delacou, B., 2007. Quaternary erosion-induced isostatic rebound in the western Alps. Geology 35(3), 195-198.

Chantraine, J., Autran, A., Cavelier, C., 1996. Geological map of France (1/1 000 000). Ed. BRGM: Orléans.

Colomb, E., Roux, R.-M., 1978. La Crau. Données nouvelles et interprétations. Géologie méditerranéenne, V(3), 303-324.

Conchon, O., 1975. Les formations quaternaires de type continental en Corse orientale. PhD thesis, Univ. Paris 6.

Conchon, O., 1977. Néotectonique en Corse orientale d'après l'étude des formations quaternaires : comparaison entre la Marana et la plaine d'Aléria. Bulletin de la Société Géologique de France 7, 631-639.

Conchon, O., 1978. Quaternary Studies in Corsica (France). Quaternary Research 9, 41-53.

Conchon, O., 1980, Stratigraphie du Quaternaire en Corse, in Chaline, J., ed., Problèmes de stratigraphie quaternaire en France et dans les pays limitrophes, AFEQ editions, 332-342.

Conchon, O., 1986. Quaternary Glaciations in Corsica. Quaternary Science Reviews 5, 429-432.

Conchon, O., 1989. Dynamique et chronologie du détritisme quaternaire en Corse, domaine méditerranéen montagnard et littoral. Bull. Asso. Fr. Et. Quat. 26(4), 201-211.

Conchon, O., 1999. Le littoral Corse au Quaternaire. Quaternaire 10, 95-105.

Crook, N., Binley, A., Knight, R., Robinson, D.A., Zarnetske, J., Haggerty, R., 2008. Electrical resistivity imaging of the architecture of substream sediments. Water Resources Research 44, W00D13, doi:10.1029/2008WR006968.

Danisik, M., Kuhlemann, J., Dunkl, I., Szekely, B., Frisch, W., 2007. Burial and exhumation of Corsica (France) in the light of fission track data. Tectonics 26, TC1001, doi:10.1029/2005TC001938.

de Boer, B., Van de Wal, R.S.W., Bintanja, R., Lourens, L.J., Tuenter, E., 2010. Cenozoic global ice-volume and temperature simulations with 1-D ice-sheet models forced by benthic d18O records. Ann. Glaciol. 51, 23–33.

Delmas, M., Braucher, R., Gunnell, Y., Guillou, V., Calvet, M., Bourlès, D., 2015. Constraints on Pleistocene glaciofluvial terrace age and related soil chronosequence features from vertical 10Be profiles in the Ariège River catchment (Pyrenees, France). Glob. Planet. Change 132, 39–53.

Delmas, M., Calvet, M., Gunnell, Y., Voinchet, P., Manel, C., Braucher, R., Tissoux, H., Bahain, J.J., Perrenoud, C., Saos, T., 2018. Terrestrial10Be and electron spin resonance dating of fluvial terraces quantifies quaternary tectonic uplift gradients in the eastern Pyrenees. Quat. Sci. Rev. 193, 188–211.

Demartini, J., Favreau, P., 2011. Référentiel Pédologique Approfondi (RPA). Caractérisation des sols de plaines et coteaux de basse altitude au 1:25.000, ODARC.

Dubar, M., 1984. Chronologie et signification des dépôts continentaux du Néogène supérieur du bassin de Riez-Valensole (Alpes-de-Haute-Provence, France). Bull. Soc. Géol. Fr (7) XXVI, 5, 971-978.

Duller, G.A.T., 1994. Luminescence dating using feldspars: a test case from southern North Island, New Zealand. Quaternary Science Reviews 13(5-7), 423-427.

Dunai, T.J., 2010. Cosmogenic Nuclides: Principles, Concepts and Applications in Earth Surface Sciences: New York, Cambridge University Press, 187 pp.

Durand, N., Gunnell, Y., Curmi, P., Ahmad, M., 2007. Pedogenic carbonates on Precambrian metamorphic rocks in South India: origin and paleoclimatic significance. Quat. Int. 162–163, 35–49.

Fan, Y.X., Zhao, H., Chen, F.H., 2010. The equivalent dose of different grain size quartz fractions from lakeshore sediments in the arid region of north China. Quaternary Geochronology 5(2-3), 205-211.

FAO, 2014. World reference base for soil resources. International soil classification system for naming soils and creating legends for soil maps. World soil resources report 106, 192 pp.

Fellin, M.G., Picotti, V., Zattin, M., 2005a. Neogene to Quaternary rifting and inversion in Corsica: Retreat and collision in the western Mediterranean. Tectonics 24, TC1011, doi:10.1029/2003TC001613.

Fellin, M.G., Zattin, M., Picotti, V., Reiners, P.W., Nicolescu, S., 2005b. Relief evolution in northern Corsica (western Mediterranean): Constraints on uplift and erosion on long-term and short-term timescales. Journal of Geophysical Research-Earth Surface 110, F01016, doi:10.1029/2004JF000167.

Fellin, M.G., Vance, J.A., Garver, J.I., Zattin, M., 2006. The thermal evolution of Corsica as recorded by zircon fission-tracks. Tectonophysics 421, 299-317.

Forzoni, A., Storms, J. E. A., Reimann, T., Moreau, J., Jouet, G., 2015. Non-linear response of the Golo River system, Corsica, France, to Late Quaternary climatic and sea level variations. Quaternary Science Reviews 121, 11-27.

Fournier, M., Jolivet, L., Goffe, B., Dubois, R., 1991. Alpine Corsica Metamorphic Core Complex. Tectonics 10, 1173-1186.

Gibbard, P. L., Head, M. J., Walker, M. J. C. and the Subcommission on Quaternary Stratigraphy. 2010. Formal ratification of the Quaternary System/Period and the Pleistocene Series/Epoch with a base at 2.58 Ma. J. Quaternary Sci. 25, 96–102.

Gosse, J.C., Phillips, F.M., 2001. Terrestrial in situ cosmogenic nuclides: theory and application. Quaternary Science Reviews 20, 1475-1560.

Gourry, J.C., Vermeersch, F., Garcin, M., Giot, D., 2003. Contribution of geophysics to the study of alluvial deposits: a case study in the Val d'Avaray area of the River Loire, France. Journal of Applied Geophysics 54, 35-49.

Granger, D.E., Kirchner, J.W., Finkel, R., 1996. Spatially averaged long-term erosion rates measured from in situ-produced cosmogenic nuclides in alluvial sediment. The Journal of Geology 104(3), 249-257.

Hancock, G.S., Anderson, R.S., Chadwick, O.A., Finkel, R.C., 1999. Dating fluvial terraces with 10Be and 26Al profiles: Application to the Wind River, Wyoming. Geomorphology 27(1-2), 41-60.

Harris, L., 1985, Progressive and Polyphase Deformation of the Schistes Lustres in Cap Corse, Alpine Corsica. Journal of Structural Geology 7, 637-650.

Herman, F., Seward, D., Valla, P.G., Carter, A., Kohn, B., Willett, S.D.,, Ehlers, T.A., 2013. Worldwide acceleration of mountain erosion under a cooling climate. Nature 504(7480), 423.

Hidy, A.J., Gosse, J.C., Pederson, J.L., Mattern, J.P., Finkel, R.C., 2010. A geologically constrained Monte Carlo approach to modeling exposure ages from profiles of cosmogenic nuclides: An example from Lees Ferry, Arizona. Geochemistry Geophysics Geosystems 11, Q0AA10, doi:10.1029/2010GC003084.

Hubschman, J., 1973. Etablissement par l'étude des faciès d'altération, d'un schéma stratigraphique du Quaternaire garonnais et ariégeois. C. R. Acad. Sci. D 277, 753–755.

Hughes, P.D., Gibbard, P.L., 2018. Global glacier dynamics during 100 ka Pleistocene glacial cycles. Quaternary Research 2018, 1-22.

Jeong, G.Y., Cheong, C.S., Choi, J.H., 2007. The effect of weathering on optically stimulated luminescence dating. Quaternary Geochronology 2(1-4), 117-122.

Kars, R.H., Wallinga, J., Cohen, K.M., 2008. A new approach towards anomalous fading correction for feldspar IRSL dating—tests on samples in field saturation. Radiation Measurements 43(2-6), 786-790.

Kars, R.H., Busschers, F.S., Wallinga, J., 2012. Validating post IR-IRSL dating on K-feldspars through comparison with quartz OSL ages. Quaternary Geochronology 12, 74-86.

Krumrei, I., 2009, Würmian glaciation and climate in the western Mediterranean based on incestigations in the mountain chain of Corsica. PhD thesis, Tübingen, Eberhard-Karls-Universität.

Kuhlemann, J., Frisch, W., Szekely, B., Dunki, I., Danisik, M., Krumrei, I., 2005. Würmian maximum glaciation in Corsica: glacier extent, amplifying paleorelief, and mesoscale climate. Austrian Journal of Earth Sciences 97, 68-81.

Kuhlemann, J., Rohling, E.J., Krumrei, I., Kubik, P., Ivy-Ochs, S., Kucera, M., 2008a, Regional synthesis of Mediterranean atmospheric circulation during the last glacial maximum. Science 321, 1338-1340.

Kuhlemann, J., van der Borg, K., Bons, P.D., Danisik, M., Frisch, W., 2008b. Erosion rates on subalpine paleosurfaces in the western Mediterranean by in-situ Be-10 concentrations in granites: implications for surface processes and long-term landscape evolution in Corsica (France): International Journal of Earth Sciences 97, 549-564.

Lahondère, J.-C., Conchon, O., Lahondère, D., 1994. Vescovato, Carte Géologique de la France, BRGM, Feuille 1107, échelle 1:50.000: Orléans, France.

Le Dortz, K., Meyer, B., Sebrier, M., Braucher, R., Bourles, D., Benedetti, L., Nazari, H., Foroutan, M., 2012. Interpreting scattered in-situ produced cosmogenic nuclide depth-profile data: Quaternary Geochronology 11, 98-115.

Legros, J. P., 2012. Major Soil Groups of the World: Ecology, Genesis, Properties and Classification. CRC Press, 447 pp.

Li, B., Li, S.H., 2011. Luminescence dating of K-feldspar from sediments: a protocol without anomalous fading correction. Quaternary Geochronology 6(5), 468-479.

Li, Y., Tsukamoto, S., Frechen, M., Gabriel, G., 2018. Timing of fluvial sedimentation in the Upper Rhine Graben since the Middle Pleistocene: constraints from quartz and feldspar luminescence dating. Boreas 47(1), 256-270.

Loke, M.H., Barker, R.D., 1996. Rapid least-squares inversion of apparent resistivity pseudosections by a quasi-Newton method, Geophysical Prospecting 44, 131-152.

Lowick, S.E., Preusser, F., 2011. Investigating age underestimation in the high dose region of optically stimulated luminescence using fine grain quartz. Quaternary Geochronology 6(1), 33-41.

Lowick, S.E., Valla, P.G., 2018. Characterising the luminescence behaviour of ‘infinitely old’quartz samples from Switzerland. Quaternary geochronology 43, 1-11.

Loÿe-Pilot, M.D., Durand-Delga, M., Feinberg, H., Gourinard, Y., Magne, J., 2004. The Burdigalian of eastern Corsica within its geodynamic setting. Comptes Rendus Geoscience 336, 919-930.

Martin, L.C.P., Blard, P.H., Balco, G., Lavé, J., Delunel, R., Lifton, N., Laurent, V., 2017. The CREp program and the ICE-D production rate calibration database: A fully parameterizable and updated online tool to compute cosmic-ray exposure ages. Quat. Geochronol. 38, 25–49. https://doi.org/10.1016/j.quageo.2016.11.006

Mattauer, M., Faure, M., Malavieille, J., 1981. Transverse Lineation and Large-Scale Structures Related to Alpine Obduction in Corsica. Journal of Structural Geology 3, 401-409.

Merchel, S., Arnold, M., Aumaitre, G., Benedetti, L., Bourlès, D.L., Braucher, R., Alfimov, V., Freeman, S.P.H.T., Steier, P., Wallner, A., 2008. Towards more precise 10Be and 36Cl data from measurements at

the 10-14 level: Influence of sample preparation. Nuclear Instruments and Methods in Physics Research B 266, 4921-4926.

Miller, K.G., Kominz, M.A., Browning, J.V., Wright, J.D., Mountain, G.S., Katz, M.E., Sugarman, P.J., Cramer, B.S., Christie-Blick, N., Pekar, S.F., 2005. The Phanerozoic record of global sea-level change. Science 310, 1293–1298.

Milner, A.M., Collier, R.E.L., Roucoux, K.H., Müller, U.C., Pross, J., Kalaitzidis, S., Christanis, K., Tzedakis, P.C., 2012. Enhanced seasonality of precipitation in the Mediterranean during the early part of the Last Interglacial. Geology 40, 919–922.

Mix, A.C., Bard, E., Schneider, R., 2001. Environmental processes of the ice age: land, oceans, glaciers (EPILOG). Quaternary Science Reviews, 20(4) 627-657.

Molliex, S., 2009. Caractérisation de la déformation tectonique récente en Provence (SE France). PhD thesis, Univ. Aix-Marseille III, 350 pp.

Molliex, S., Siame, L., Bourlès, D.L., Braucher, R., Bellier, O., Clauzon, G., 2013. Quaternary evolution of a large alluvial fan in a peri-glacial setting (Crau plain, SE France), constrained by terrestrial cosmogenic nuclide (10Be). Geomorphology 195, 45–52.

Molliex, S., Jouet, J., Freslon, N., Bourlès, D.L., Authemayou, C., Moreau, J., Rabineau, M., 2017. Controls on Holocene denudation rates in mountainous environments under Mediterranean climate. Earth Surface Processes and Landforms 42(2), 272-289. doi: 10.1002/esp.3987

Muscheler, R., Beer, J., Kubik, P.W., Synal, H.A., 2005. Geomagnetic field intensity during the last 60,000 years based on10Be and36Cl from the Summit ice cores and14C. Quat. Sci. Rev. 24, 1849–1860. https://doi.org/10.1016/j.quascirev.2005.01.012

Nishiizumi, K., 2004. Preparation of 26Al AMS standards. Nuclear Instruments and Methods in Physics Research Section B: Beam Interactions with Materials and Atoms 223, 388-392.

Nishiizumi, K., Imamura, M., Caffee, M. W., Southon, J. R., Finkel, R. C., McAninch, J., 2007. Absolute calibration of 10Be AMS standards. Nuclear Instruments and Methods in Physics Research Section B: Beam Interactions with Materials and Atoms 258(2), 403-413.

Pedoja, K., Husson, L., Regard, V., Cobbold, P.R., Ostanciaux, E., Johnson, M.E., Kershaw S., Saillard, M., Martinod, J. Furgerot, L., Weill, P., Delcaillau, B., 2011. Relative sea-level fall since the last interglacial stage: are coasts uplifting worldwide? Earth-Science Reviews 108(1-2), 1-15.

Pedro, G., 1968. Distribution des principaux types d'altération chimique à la surface du globe. Présentation d'une esquisse géographique: Revue de Géographie Physique et Géologie Dynamique 10, 457-470.

Petit, C., Campy, M., Chaline, J., Bonvalot, J., 1996. Major palaeohydrographic changes in Alpine foreland during the Pliocene-Pleistocene. Boreas 25(2), 131-143.

Peyron, O., Guiot, J., Cheddadi, R., Tarasov, P., Reille, M., de Beaulieu, J.L., Bottema, S., Andrieu, V., 1998. Climatic reconstruction in Europe for 18,000 yr B.P. from pollen data. Quaternary Research 49, 183-196.

Reille, M., Gamisans, J., deBeaulieu, J.L., Andrieu, V., 1997. The late-glacial at Lac de Creno (Corsica, France): A key site in the western Mediterranean Basin. New Phytologist 135, 547-559.

Reille, M., Gamisans, J., Andrieu-Ponel, V., De Beaulieu, J.-L., 1999. The Holocene at Lac de Creno, Corsica, France : a key site for the whole island. New Phytologist 141, 291–307.

Reimann, T., Román-Sánchez, A., Vanwalleghem, T., & Wallinga, J., 2017. Getting a grip on soil reworking–Single-grain feldspar luminescence as a novel tool to quantify soil reworking rates. Quaternary Geochronology 42, 1-14.

Rohling, E.J., 1994. Review and new aspects concerning the formation of eastern Mediterranean sapropels. Mar. Geol. 122, 1–28.

Rohling, E.J., Foster, G.L., Grant, K.M., Marino, G., Roberts, A.P., Tamisiea, M.E., Williams, F., 2014. Sea-level and deep-sea-temperature variability over the past 5.3 million years. Nature 508(7497), 477–482.

Rohling, E.J., Marino, G., Grant, K.M., 2015. Mediterranean climate and oceanography, and the periodic development of anoxic events (sapropels). Earth-Science Rev. 143, 62–97.

Saint-Carlier, D., Charreau, J., Lavé, J., Blard, P.H., Dominguez, S., Avouac, J.P., Wang, S., Arnold, M., Aumaître, G., Keddadouche, K., Léanni, L., Chauvet, F., Bourlés, D.L., 2016. Major temporal variations in shortening rate absorbed along a large active fold of the southeastern Tianshan piedmont (China). Earth Planet. Sci. Lett. 434, 333–348.

Sasaki, Y., 1992. Resolution of resistivity tomography inferred from numerical simulation. Geophysical Prospecting 40, 453-464.

Serrano, O., Allanic, C., Magar, M., 2013. Synthèse géologique du bassin tertiaire de la plaine orientale corse. Liaison terre-mer entre Nicolao et Solenzara. BRGM report RP62303FR. 181 pp.

Siame, L., Bellier, O., Braucher, R., Sebrier, M., Cushing, M., Bourles, D., Hamelin, B., Baroux, E., de Voogd, B., Raisbeck, G., Yiou, F., 2004. Local erosion rates versus active tectonics: cosmic ray exposure modelling in Provence (south-east France). Earth and Planetary Science Letters 220, 345-364.

Skyles, E.M., 2013, Alluvial geochronology and watershed analysis of the Golo River, Northeastern Corsica, France. Msc thesis, Logan, Utah State University.

Sømme, T.O., Piper, D.J.W., Deptuck, M.E., Helland-Hansen, W., 2011. Linking Onshore-Offshore Sediment Dispersal in the Golo Source-to-Sink System (Corsica, France) during the Late Quaternary. Journal of Sedimentary Research 81, 118-137.

Spratt, R.M., Lisiecki, L.E., 2016. A Late Pleistocene sea level stack. Clim. Past 12, 1079–1092.

Steffen, D., Preusser, F., Schlunegger, F., 2009. OSL quartz age underestimation due to unstable signal components. Quaternary Geochronology 4(5), 353-362.

Stone, J.O., 2000, Air pressure and cosmogenic isotope production. Journal of Geophysical Research-Solid Earth 105, 23753-23759.

Sweet, M.L., Gaillot, G.T., Jouet, G., Rittenour, T.M., Toucanne, S., Marsset, T., Blum, M.D., 2020. Sediment routing from shelf to basin floor in the Quaternary Golo System of Eastern Corsica, France, western Mediterranean Sea. Geological Society of America Bulletin 132 (5-6): 1217–1234.

Thiel, C., Buylaert, J. P., Murray, A., Terhorst, B., Hofer, I., Tsukamoto, S., Frechen, M., 2011. Luminescence dating of the Stratzing loess profile (Austria)–Testing the potential of an elevated temperature post-IR IRSL protocol. Quaternary International 234(1-2), 23-31

Timar, A., Vandenberghe, D., Panaiotu, E. C., Panaiotu, C. G., Necula, C., Cosma, C., 2010. Optical dating of Romanian loess using fine-grained quartz. Quaternary Geochronology, 5(2-3) 143-148.

Timar-Gabor, A., Buylaert, J.P., Guralnik, B., Trandafir-Antohi, O., Constantin, D., Anechitei-Deacu, V., Jain, M., Murray, A.S, Porat, N., Hao, Q., Wintle, A.G., 2017. On the importance of grain size in luminescence dating using quartz. Radiation Measurements 106, 464-471.

Toucanne, S., Minto'o, C. M. A., Fontanier, C., Bassetti, M. A., Jorry, S. J., Jouet, G., 2015. Tracking rainfall in the northern Mediterranean borderlands during sapropel deposition. Quaternary Science Reviews 129, 178-195.

Twidale, CR., 2004. River patterns and their meaning. Earth-Science Reviews 67(3-4), 159-218.

Uppala, S.M., Kållberg, P.W., Simmons, A.J., Andrae, U., da Costa Bechtold, V., Fiorino, M., Gibson, J.K., Haseler, J., Hernandez, A., Kelly, G.A., Li, X., Onogi, K., Saarinen, S., Sokka, N., Allan, R.P., Andersson, E., Arpe, K., Balmaseda, M.A., Beljaars, A.C.M., van de Berg, L., Bidlot, J., Bormann, N., Caires, S., Chevallier, F., Dethof, A., Dragosavac, M., Fisher, M., Fuentes, M., Hagemann, S., Hólm, E., Hoskins, B.J., Isaksen, L., Janssen, P.A.E.M., Jenne, R., McNally, A.P., Mahfouf, J.F., Morcrette, J.J., Rayner, N.A., Saunders, R.W., Simon, P., Sterl, A., Trenberth, K.E., Untch, A., Vasiljevic, D., Viterbo, P., Woollen, J., 2005. The ERA-40 re-analysis. Q. J. R. Meteorol. Soc. 131, 2961–3012. https://doi.org/10.1256/qj.04.176

Valla, PG., Shuster, DL., Van Der Beek, PA., 2011. Significant increase in relief of the European Alps during mid-Pleistocene glaciations. Nature geoscience 4(10), 688.

Vreeken, W.J., 1975. Principal kinds of chronosequences and their significance in soil his tory. J. Soil Sci. 26, 378–394.

Wintle, A.G. 1973. Anomalous fading of thermo-luminescence in mineral samples. Nature 245(5421), 143-144.

FIGURE CAPTIONS

1) Geomorphological and geological setting of the Golo River catchment (modified from Molliex et al., 2017). A) Topographic map. B) Geological map (from Chantraine et al., 1996). LGM glaciers extent from Kuhlemann et al., (2005).

2) Morphologic map of the Golo alluvial plain. Morphological areas are defined on the basis of slope breaks. Locations of topographic and soil-related profiles of Fig.3.

3) Topographic profiles of the Golo alluvial plain (location in Fig. 2), with soil related correspondence. A) A-B-C-D profiles are West-East oriented (longitudinally to Golo present-day Valley); B) E-F-G profiles are South-North oriented (transversally to the Golo present-day Valley). C) Relationship between elevation and slope of each pixel of the plain according to the type of soil and the definition of morphologic areas (Upper, Middle and Lower plain). In the three sub-figures, morphological areas are represented by the grey-scale background.

4) Classification of alluvial soils of the Golo alluvial plain. A) Synthetic typical logs from the different terraces of the Golo alluvial plain. B) Pictures illustrating the typical types of soils from the Golo alluvial plain terraces. C) Relative abundance of soil evolution weathering processes for each terrace. Modified from Demartini and Favreau (2011).

5) Updated geological map of Quaternary formations of the Golo coastal plain, based on morphology, sedimentology and soil characteristics. The black dashed line shows the extent of Golo deposits. Insert in top right corner represent the location of soil data from Demartini and Favreau (2011).

6) Gol10 (A) and Gol06 (B) Electrical Resistivity Image (ERI) and interpretations obtained with a Schlumberger protocol, 64 electrodes, 10m-spacing, 630 m- and 950 m-long, respectively, with a 90m-deep penetration. Interpretations are based on surface geology, borehole data and contrasts of resistivity. Location of profiles is indicated in Fig. 5.

7) A) GBEC5-2 lithologic and stratigraphic log. (X = 9.45532°E; Y = 42.52767°N; Z = 18 m, location on Fig. 5) B) Statistics on pebbles content along the GBEC5-2 borehole. C) Some representative pictures of each formation, with true color and scale.

8) Cosmogenic ^{10}Be dating of the Fy2 terrace at the CICO gravel pit (location on Fig. 5). A - Picture of the Fy2 CICO gravel pit outcrop showing the samples analyzed for in situ cosmogenic ^{10}Be. B - Measured cosmogenic ^{10}Be concentration in quartz (at.g $^{-1}$) vs sampling depth. Red curve is the modeled best-fit attenuation profile, including production by spallation and muons. Used parameters are: a world average SLHL production rate of 4.13 ± 0.20 at.g $^{-1}$ .yr $^{-1}$ (CREp calculator; Martin et al., 2017), with the Lal/Stone time dependent scaling (Stone, 2000; Balco et al., 2008), the ERA40 atmosphere (Uppala et al., 2005) and the geomagnetic reconstruction of Muscheler et al., 2005. Muonic production is modeled with the exponential attenuation profile and the parameters defined in (Braucher et al., 2011). C - Most probable exposure erosion solutions represented as Khi-2 values for variable erosion and exposure time couples. These estimates are obtained using the Monte Carlo best-fit modeling approach of Saint-Carlier et al. (2016). This algorithm is a development of the (Hidy et al., 2010) model that takes into account the stochastic variability and the uncertainty of the inherited component. Our inversion shows that the ^{10}Be profile requires a minimum exposure duration of 70 ka and a maximum denudation rate of 10 ± 2 mm.ka^{-1}. D - Estimate of the inherited ^{10}Be component.

9) Photos of luminescence IRSL sample sites. A1) CICO Fy2 terrace site. A2) Zoom on the CICO sample zone. The black arrows show bioturbations in sediment caused by rooted vegetation. B1) SINI Fy1 terrace site. B2) Zoom on the SINI sample zone. White squares on A1 and B1 correspond to the extent of photo A2 and B2 respectively. CICO and SINI samples position can be found in Fig. 5 and Table 4.

10) Interpretation of GBEC5-2 borehole in its geological setting. A) Outcrop of the base of the highest Quaternary terrace (Fy1) just upstream of the alluvial plain (location in B). B) Local geological map of GBEC5-2 setting. C) Longitudinal profile of Golo River and geological interpretative cross-section. D) Picture of the base of GBEC5 borehole, showing alluvial braided material at 117.4 m below ground floor.

TABLE CAPTIONS

1) Characteristics of Golo alluvial terraces with a comparison of estimated published ages

2) ^{10}Be data along the depth profile of CICO gravel pit (X = 9.4878°E; Y = 42.5495°N, Z = 6 m) (location in Fig. 5). The measured blank ^{10}Be/^{9}Be ratio is (4.40 ± 1.97) x 10^{-16}. Age interpretations are presented in Fig. 8.

3) ^{26}Al/^{10}Be raw data and burial durations for the samples of the borehole GBEC5. The Matlab© code and the parameters summarized in (Blard et al., 2019) were used to compute the ^{26}Al/^{10}Be burial ages, with a catchment mean altitude of pre-burial exposure of 926 m, similar to present-day. Note that ^{10}Be concentration has been measured both at ASTER and PRIME Lab AMS. ^{9}Be (at) is the amount of added carrier, while ^{27}Al (at) corresponds to the sum of the natural ^{27}Al (at) measured in the sample and the amount of added carrier. Blank ^{10}Be/^{9}Be ratio for ASTER measurements is (1.94 ± 0.54) x 10^{-15}. Blank ^{10}Be/^{9}Be ratio for PRIME lab measurements is (0.65 ± 0.75) x 10^{-15}. Blank ^{26}Al/^{27}Al ratio is (1.45 ± 1.39) x 10^{-15}. The interlaboratory comparison of ^{10}Be concentrations shows an agreement within uncertainties. Bold data corresponds to ^{26}Al/^{10}Be with the lowest uncertainties and are the age retained in our interpretations. Italic data correspond to ratio with higher uncertainties.

4) Synthesis of published OSL/IRSL data in the Golo alluvial plain.

Geologic Map Unit (BRGM)	Alernative nomenclature	Type of soil associated	Electrical Resistivity ($\Omega.m^{-1}$)		
				Conchon, 1989	Somme
Fz	N7	Row Fluvisol	120-250	1	
Fy3	N6	Typical Fluvisol	300-800	2	
Fy2	N5	Brown Soil	350-800	3	
Fy1	N4	Reddish Brown Soil	240-600	4	
Fx	N3	Luvisol	-	6	
Fw	N2	Ferralsol	80-350	8	
Fv	N1	-	10-80	10	

Sample name	Depth (cm)	Mass of dissolved Quartz (g)	$^{10}Be/^{9}Be$ ($x\ 10^{-14}$)	^{9}Be ($x10^{19}$ at)	^{10}Be $x10^{4}$ at.g$(SiO_2)^{-1}$
CICO 0	0	20.13	13.173 ± 0.592	2.022	28.09 ± 1.82
CICO 25	25	14.31	9.573 ± 0.371	2.024	28.73 ± 1.75
CICO 52	52	21.07	8.395 ± 0.383	2.010	17.00 ± 1.10
CICO 70	70	7.87	4.444 ± 0.219	2.031	24.27 ± 1.65
CICO 95	95	20.01	6.169 ± 0.818	2.027	13.25 ± 1.87
CICO 140	140	20.43	4.951 ± 0.428	2.033	10.43 ± 1.03
CICO 185	185	20.38	4.300 ± 0.347	2.025	9.04 ± 0.81
CICO 200	200	20.61	6.879 ± 0.256	2.056	14.56 ± 0.87
CICO 263	263	20.32	2.656 ± 0.222	2.034	5.61 ± 0.54
CICO 300	300	20.20	2.009 ± 0.281	2.042	4.27 ± 0.34
CICO 490	490	20.28	1.729 ± 0.207	2.042	3.66 ± 0.45

Name	GBEC5-2 Depth (m)	Mass of dissolved quartz (g)	$^{10}Be/^{9}Be$ Ratio ($x10^{15}$)	^{9}Be ($x10^{19}$ at)	^{10}Be $x10^{4}$ at.$g^{-1}(SiO_{2})$	AMS	$^{26}Al/^{27}Al$ Ratio ($x10^{15}$)	^{27}Al ($x10^{19}$ at)	^{26}Al $x10^{4}$ at.$g(SiO2)^{-1}$	$^{26}Al/^{10}Be$ ratio	Burial duration (Ma)
B5 S59	**37.8**	**9.888**	**23.410 ± 2.268**	**2.310**	**4.89 ± 0.47**	**ASTER**	**10.74 ± 2.88**	**2.243**	**10.75 ± 3.32**	**2.198 ± 0.711**	**2.45 ± 0.73**
B5 S59	*37.8*	*3.119*	*7.950 ± 1.710*	*1.711*	*4.00 ± 1.02*	*PRIME Lab*	*10.74 ± 2.88*	*2.243*	*10.75 ± 3.32*	*2.689 ± 1.077*	*1.94 ± 0.89*
B5 S145	*116.5*	*11.144*	*16.6 ± 2.227*	*2.310*	*2.93 ± 0.39*	*ASTER*	*7.391 ± 1.965*	*2.213*	*7.43 ± 2.46*	*2.535 ± 0.906*	*2.15 ± 0.80*
B5 S145	**116.5**	**3.090**	**7.839 ± 1.793**	**1.711**	**3.97 ± 1.07**	**PRIME Lab**	**7.391 ± 1.965**	**2.213**	**7.43 ± 2.46**	**1.870 ± 0.799**	**2.74 ± 0.95**

Sample Name	Lat. (N)	Long. (E)	Terrace	Depth (m)	Method	Absolute age	Reference
NCL-5212119	42°33'15.468"	9°29'05.874"	Fy2-CICO	2.00	$pIRIR_{290}$	43 ± 4 ka	Forzoni et al., 2015
NCL-5212120	42°33'17.581"	9°29'05.025"	Fy2-CICO	2.10	$pIRIR_{290}$	46 ± 7 ka	Forzoni et al., 2015
NCL-5212118	42°31'15.269"	9°27'38.805"	Fy1-SINI	4.10	$pIRIR_{290}$	92 ± 11 ka	Forzoni et al., 2015
NCL-5212116	42°31'15.269"	9°27'38.805"	Fy1-SINI	4.30	$pIRIR_{290}$	100 ± 12 ka	Forzoni et al., 2015
Golo 6A	42°30'52.759"	9°27'01.337"	Fw	2.00	OSL	45 ± 3 ka	Somme et al., 2011
Golo 6B	42°30'52.759"	9°27'01.337"	Fw	2.00	OSL	76 ± 5 ka	Somme et al., 2011

Dr. Stéphane Molliex
Laboratoire Géosciences Océan
IUEM, UMR 6538
Place N. Copernic
F-29280 Plouzané
France
Tel: +33 2 98 8910 04
Email: smolliex@gmail.com

Editor of *Quaternary Geochronology*

Subject: Submission of a manuscript to "*Quaternary Geochronology*"

Dear Editor,

We declare that we have no conflict of interest in the research called *"Revisiting extent and chronology of the Golo River alluvial plain deposits (NE Corsica, France)."* by S. Molliex and co-authors that we submit for consideration of publication in Quaternary Geochronology. Please note nevertheless that an associate editor of Quaternary Geochronology (P.-H. Blard) is co-author of this work.

Best Regards,

Dr. Stéphane Molliex on behalf of all co-authors

Figure 1

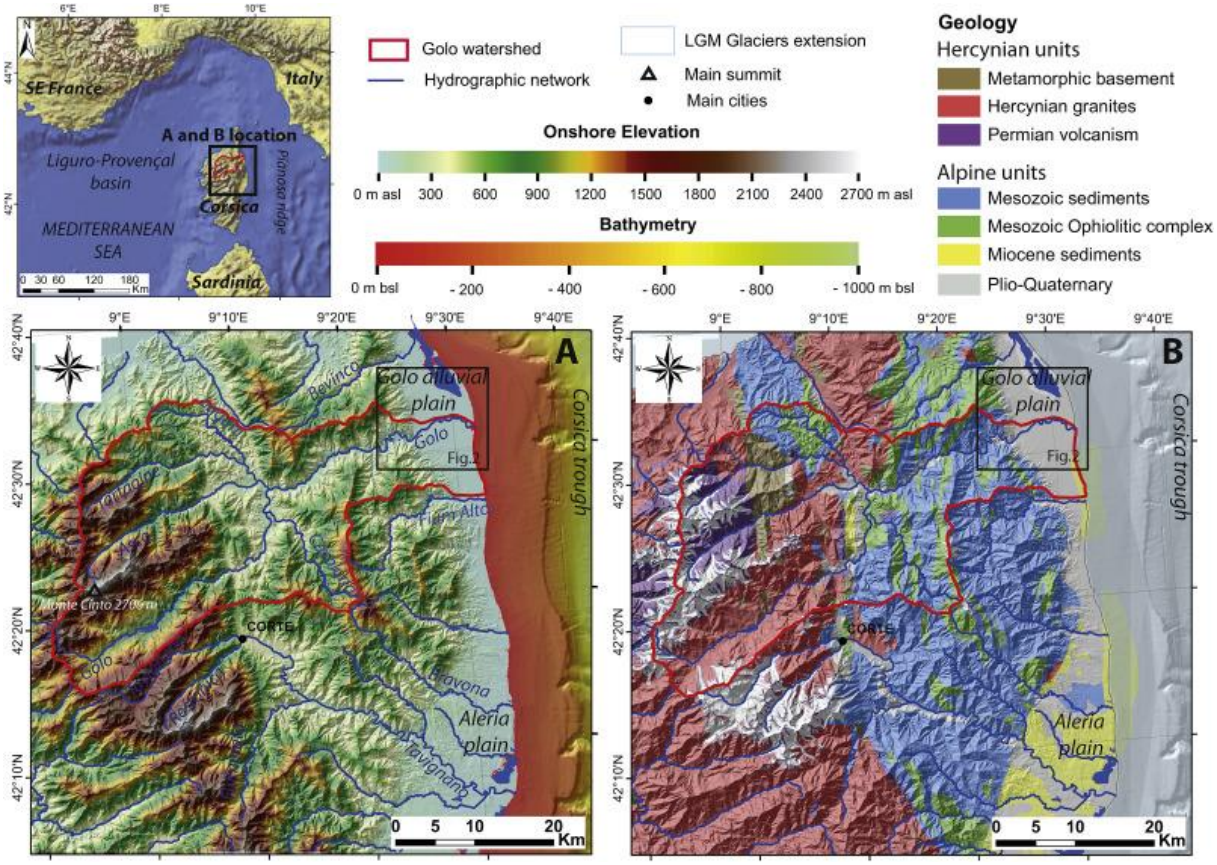
SE France
Italy
A and B location
Liguro-Provençal basin
Corsica
Pianosa ridge
MEDITERRANEAN SEA
Sardinia
Golo watershed
Hydrographic network
LGM Glaciers extension
Main summit
Main cities
Onshore Elevation
0 m asl 300 600 900 1200 1500 1800 2100 2400 2700 m asl
Bathymetry
0 m bsl - 200 - 400 - 600 - 800 - 1000 m bsl
Geology
Hercynian units
Metamorphic basement
Hercynian granites
Permian volcanism
Alpine units
Mesozoic sediments
Mesozoic Ophiolitic complex
Miocene sediments
Plio-Quaternary
A
B
Golo alluvial plain
Fig.1
Fig.2
Corsica trough
Bevinco
Golo
Fiumalto
Monte Cinto 2706 m
CORTE
Bravona
Aleria plain
Tavignano
0 5 10 20 Km

Figure 2

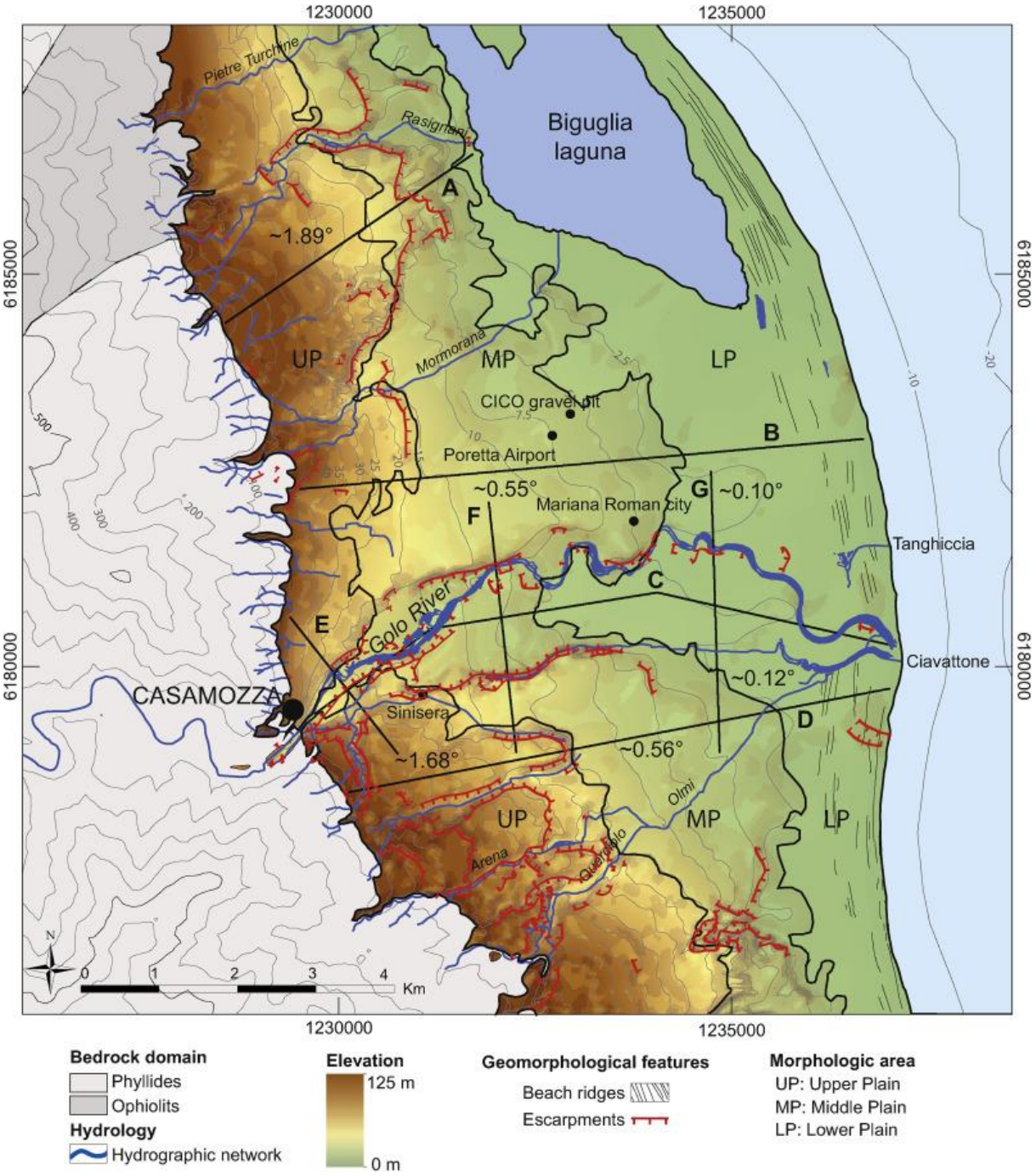
1230000
1235000
6185000
6180000
Pietre Turchine
Rasignano
Biguglia laguna
A
~1.89°
UP
Mormorana
MP
LP
CICO gravel pit
Poretta Airport
B
~0.55°
Mariana Roman city
G
~0.10°
F
Tanghiccia
C
Golo River
E
Ciavattone
~0.12°
CASAMOZZA
Sinisera
D
~1.68°
~0.56°
Olmi
UP
MP
LP
Arena
Quercitello
N
0
1
2
3
4
Km
Bedrock domain
Phyllides
Ophiolits
Hydrology
Hydrographic network
Elevation
125 m
0 m
Geomorphological features
Beach ridges
Escarpments
Morphologic area
UP: Upper Plain
MP: Middle Plain
LP: Lower Plain

Figure 3

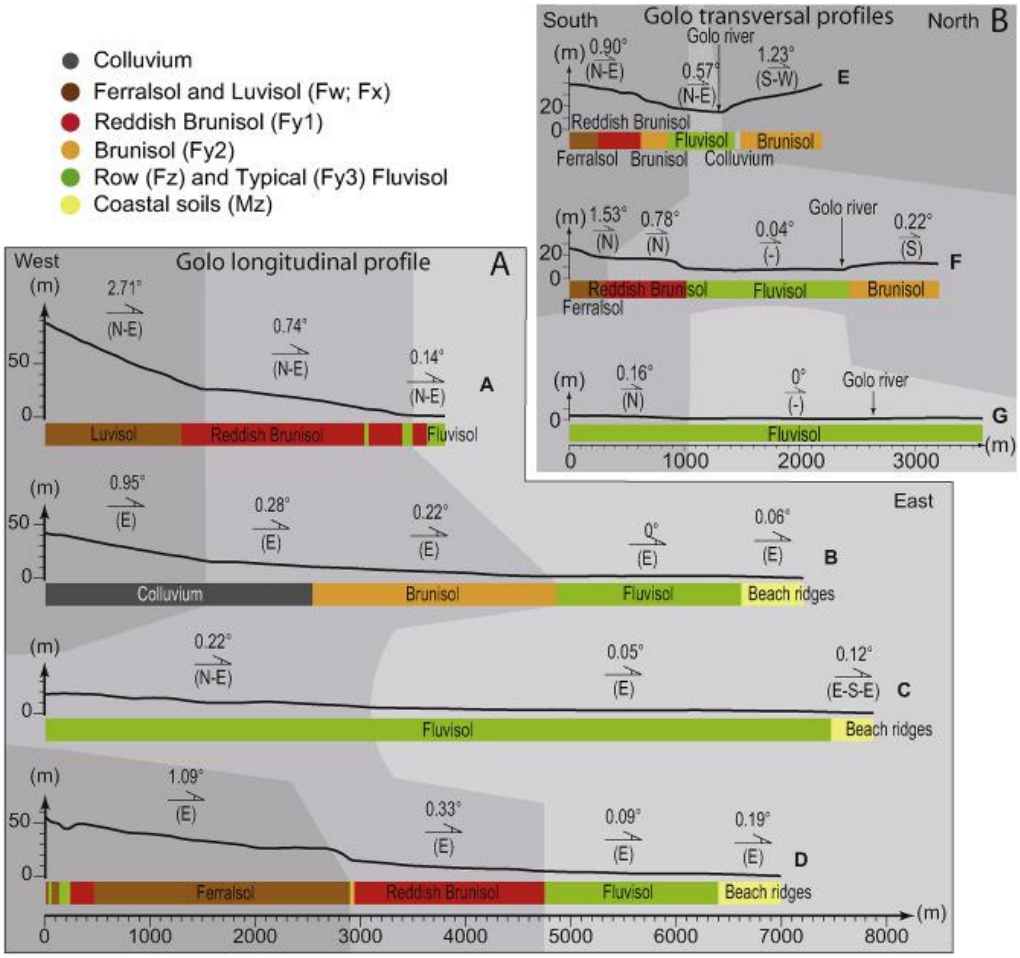
Colluvium
Ferralsol and Luvisol (Fw; Fx)
Reddish Brunisol (Fy1)
Brunisol (Fy2)
Row (Fz) and Typical (Fy3) Fluvisol
Coastal soils (Mz)
Golo longitudinal profile
West
East
A
B
C
D
Luvisol
Reddish Brunisol
Fluvisol
Colluvium
Brunisol
Beach ridges
Ferralsol
Golo transversal profiles
South
North
Golo river
E
F
G
Reddish Brunisol
Fluvisol
Brunisol
Ferralsol
Colluvium

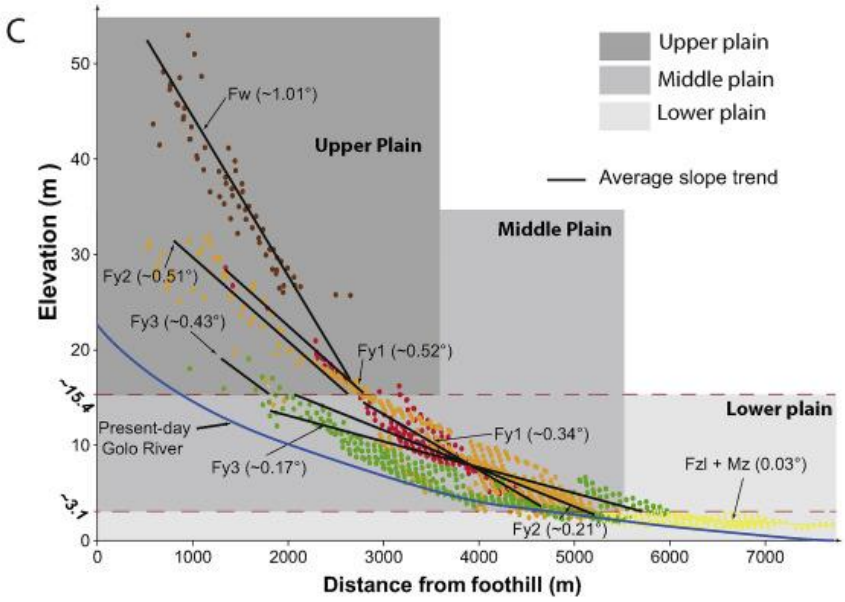
C
Upper plain
Middle plain
Lower plain
Average slope trend
Fw (~1.01°)
Upper Plain
Middle Plain
Lower plain
Fy2 (~0.51°)
Fy3 (~0.43°)
Fy1 (~0.52°)
Present-day
Golo River
Fy3 (~0.17°)
Fy1 (~0.34°)
Fzl + Mz (0.03°)
Fy2 (~0.21°)
Elevation (m)
Distance from foothill (m)

Figure 4

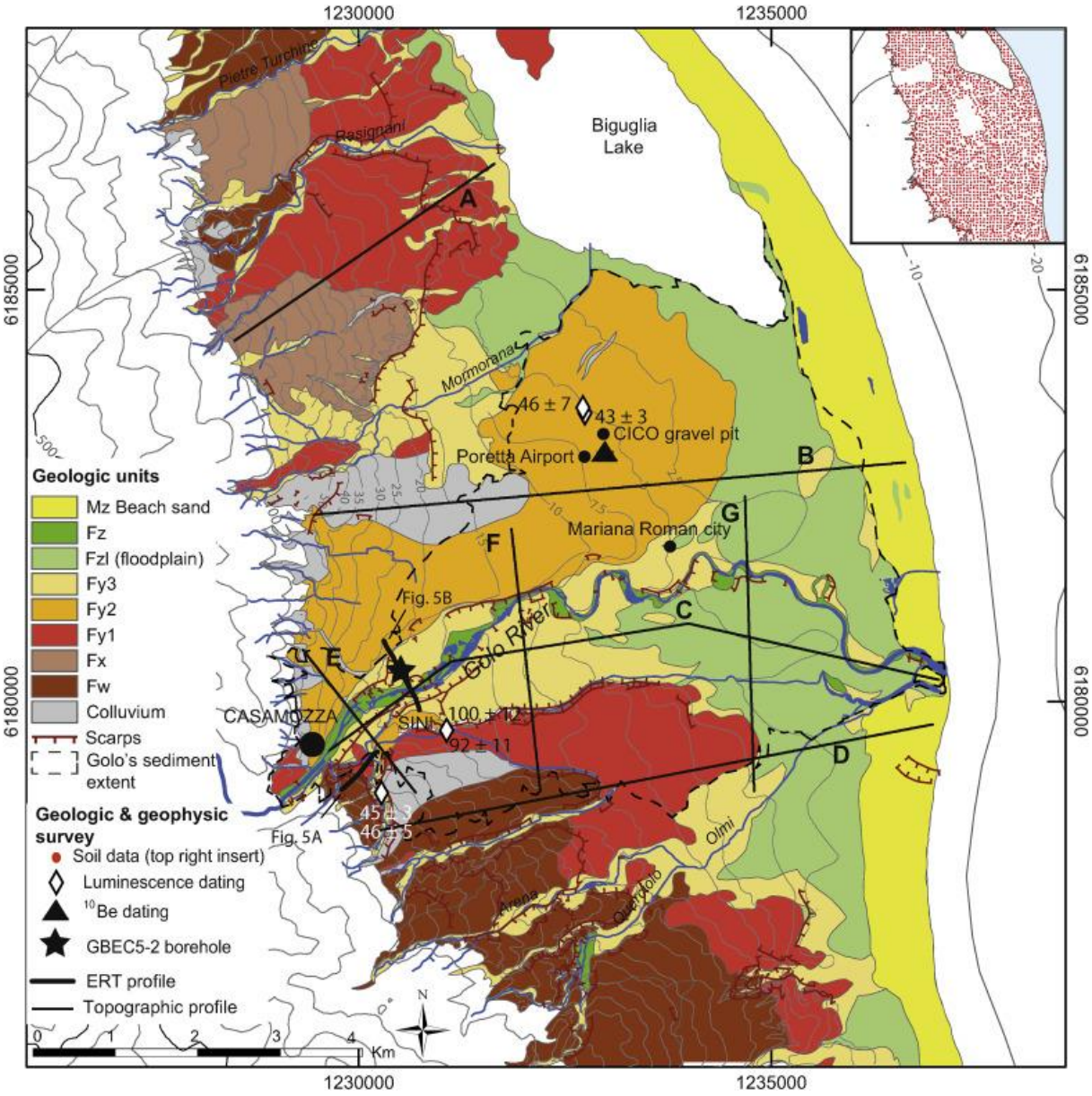
1230000
1235000
6185000
6180000
Biguglia Lake
Pietre Turchine
Rasignani
Mormorana
46 ± 7
43 ± 3
CICO gravel pit
Poretta Airport
Mariana Roman city
Fig. 5B
Golo River
CASAMOZZA
SINI
100 ± 12
92 ± 11
45 ± 3
46 ± 5
Fig. 5A
Olmi
Arena
Querciolo
A
B
C
D
E
F
G
Geologic units
Mz Beach sand
Fz
Fzl (floodplain)
Fy3
Fy2
Fy1
Fx
Fw
Colluvium
Scarps
Golo's sediment extent
Geologic & geophysic survey
Soil data (top right insert)
Luminescence dating
10Be dating
GBEC5-2 borehole
ERT profile
Topographic profile
0 1 2 3 4 Km
N

Figure 5

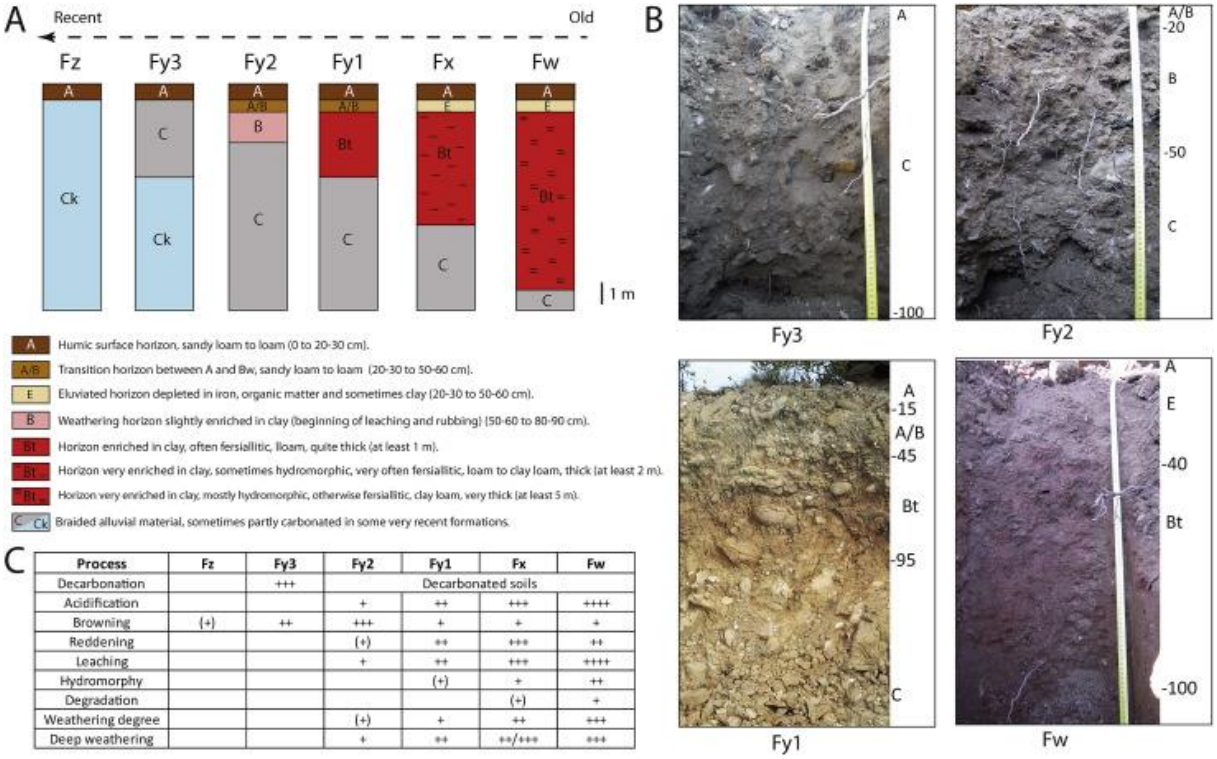

C

Process	Fz	Fy3	Fy2	Fy1	Fx	Fw
Decarbonation		+++	Decarbonated soils			
Acidification			+	++	+++	++++
Browning	(+)	++	+++	+	+	+
Reddening			(+)	++	+++	++
Leaching			+	++	+++	++++
Hydromorphy				(+)	+	++
Degradation					(+)	+
Weathering degree			(+)	+	++	+++
Deep weathering			+	++	++/+++	+++

Figure 6

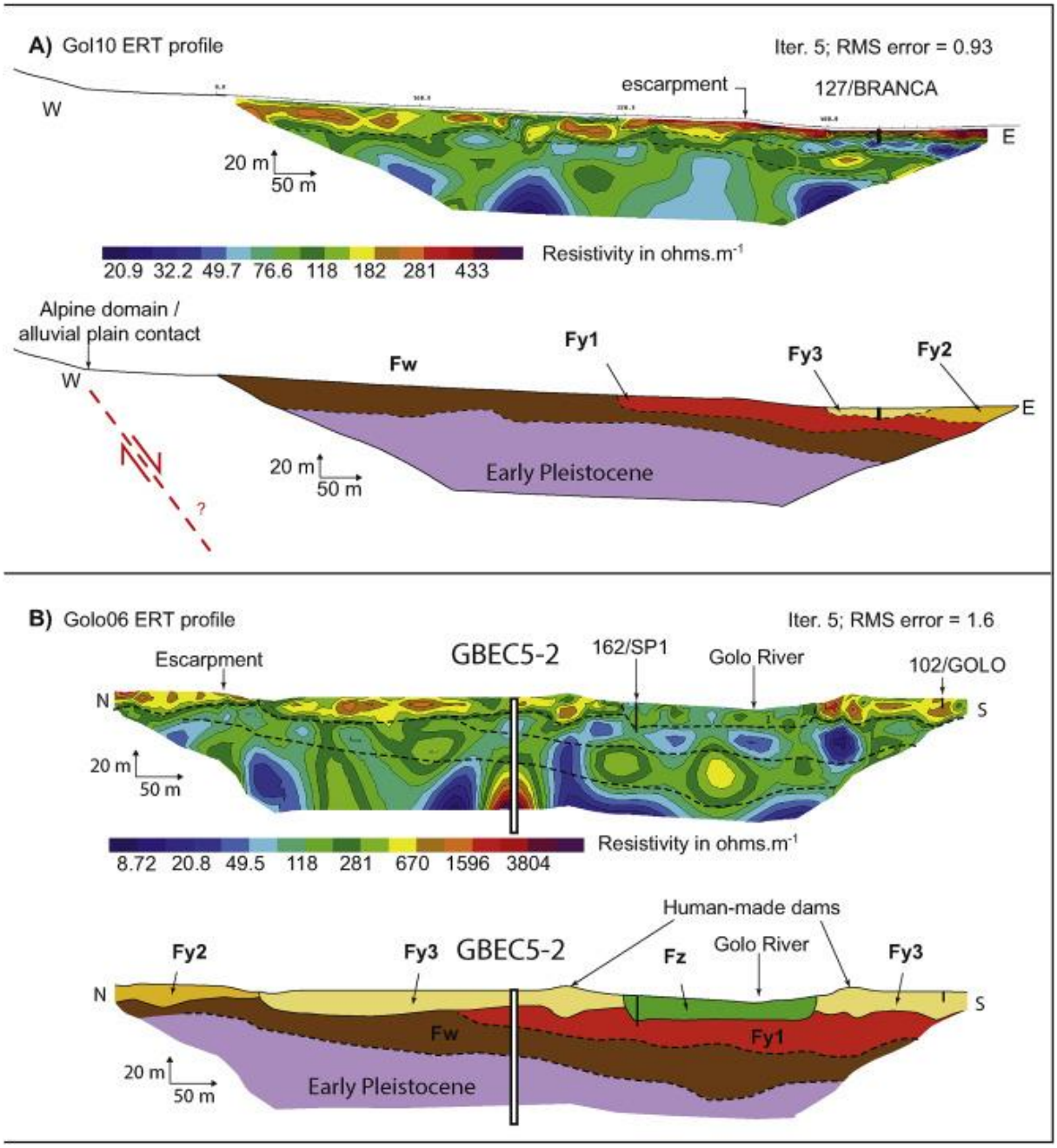
A) Gol10 ERT profile
Iter. 5; RMS error = 0.93
escarpment
127/BRANCA
W
E
20 m
50 m
20.9 32.2 49.7 76.6 118 182 281 433
Resistivity in ohms.m-1
Alpine domain / alluvial plain contact
Fw
Fy1
Fy3
Fy2
W
E
20 m
50 m
Early Pleistocene
?
B) Golo06 ERT profile
Iter. 5; RMS error = 1.6
Escarpment
GBEC5-2
162/SP1
Golo River
102/GOLO
N
S
20 m
50 m
8.72 20.8 49.5 118 281 670 1596 3804
Resistivity in ohms.m-1
Human-made dams
Fy2
Fy3
GBEC5-2
Fz
Golo River
Fy3
N
S
Fw
Fy1
20 m
50 m
Early Pleistocene

Figure 7

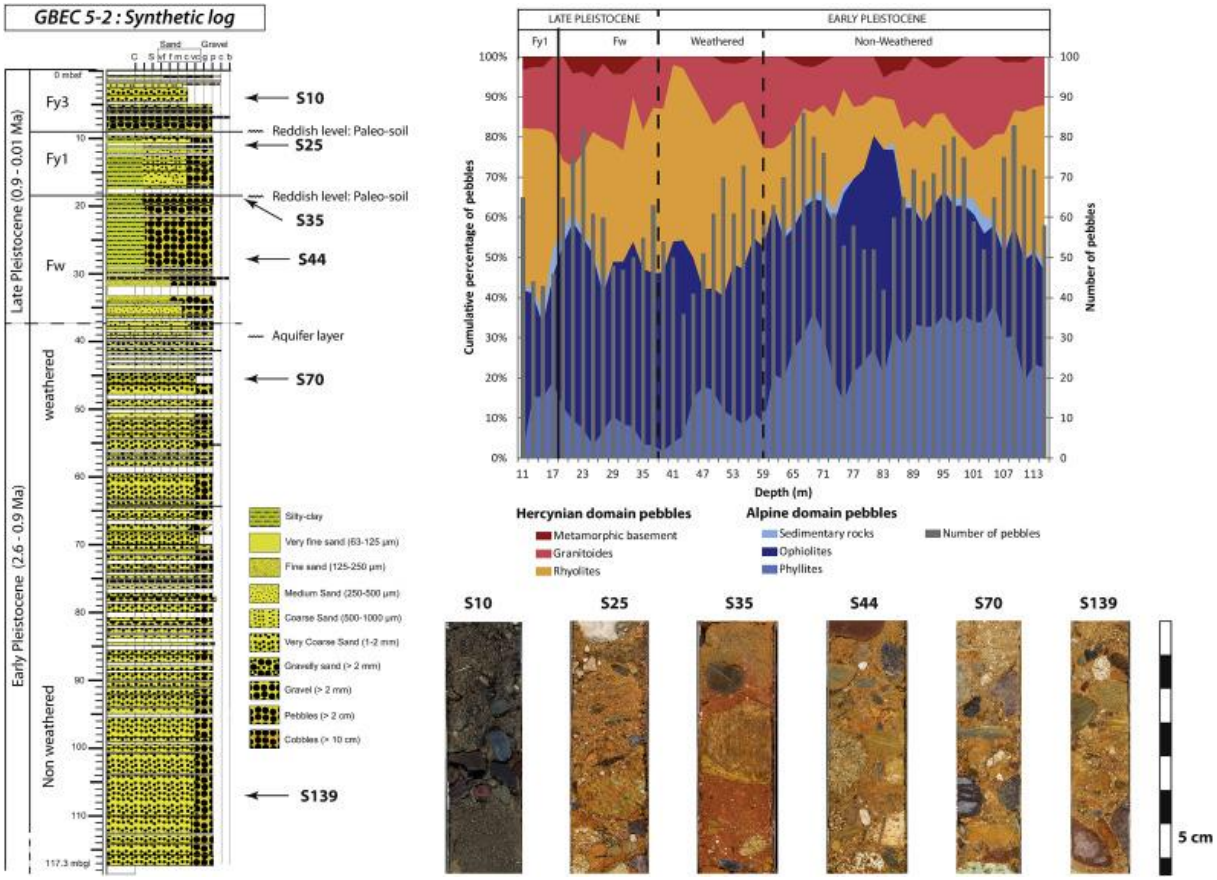
GBEC 5-2 : Synthetic log
Late Pleistocene (0.9 - 0.01 Ma)
Early Pleistocene (2.6 - 0.9 Ma)
Fy3
Fy1
Fw
weathered
Non weathered
S10
Reddish level: Paleo-soil
S25
Reddish level: Paleo-soil
S35
S44
Aquifer layer
S70
S139
Silty-clay
Very fine sand (63-125 µm)
Fine sand (125-250 µm)
Medium Sand (250-500 µm)
Coarse Sand (500-1000 µm)
Very Coarse Sand (1-2 mm)
Gravelly sand (> 2 mm)
Gravel (> 2 mm)
Pebbles (> 2 cm)
Cobbles (> 10 cm)
LATE PLEISTOCENE
EARLY PLEISTOCENE
Fy1
Fw
Weathered
Non-Weathered
Cumulative percentage of pebbles
Number of pebbles
Depth (m)
Hercynian domain pebbles
Metamorphic basement
Granitoides
Rhyolites
Alpine domain pebbles
Sedimentary rocks
Ophiolites
Phyllites
Number of pebbles
S10
S25
S35
S44
S70
S139
5 cm

Figure 8

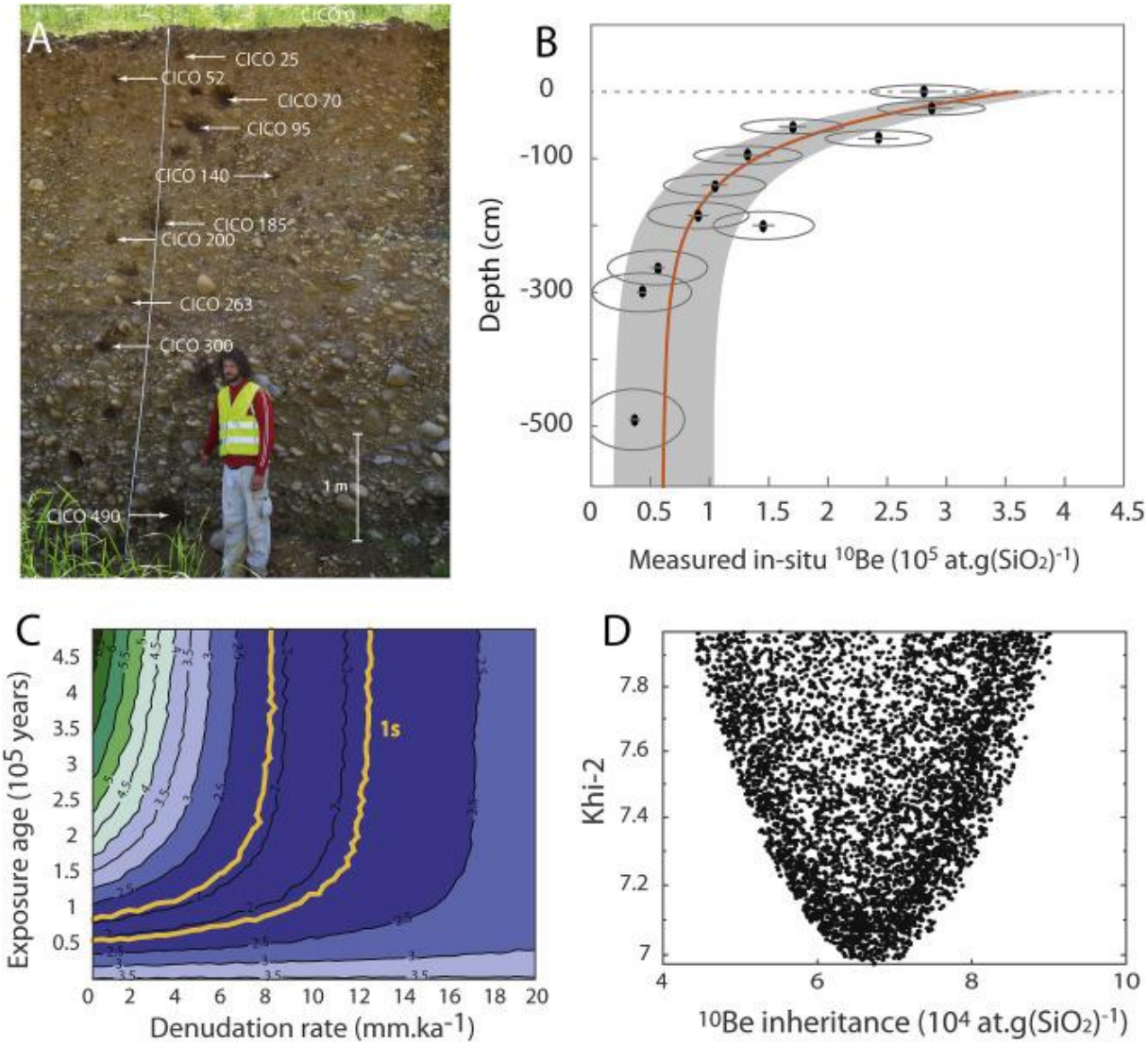
A
CICO 0
CICO 25
CICO 52
CICO 70
CICO 95
CICO 140
CICO 185
CICO 200
CICO 263
CICO 300
CICO 490
1 m
B
Depth (cm)
0
-100
-300
-500
0 0.5 1 1.5 2 2.5 3 3.5 4 4.5
Measured in-situ ^{10}Be (10^5 at.g(SiO_2)$^{-1}$)
C
Exposure age (10^5 years)
4.5 4 3.5 3 2.5 2 1.5 1 0.5
1s
0 2 4 6 8 10 12 14 16 18 20
Denudation rate (mm.ka^{-1})
D
Khi-2
7.8 7.6 7.4 7.2 7
4 6 8 10
^{10}Be inheritance (10^4 at.g(SiO_2)$^{-1}$)

Figure 9

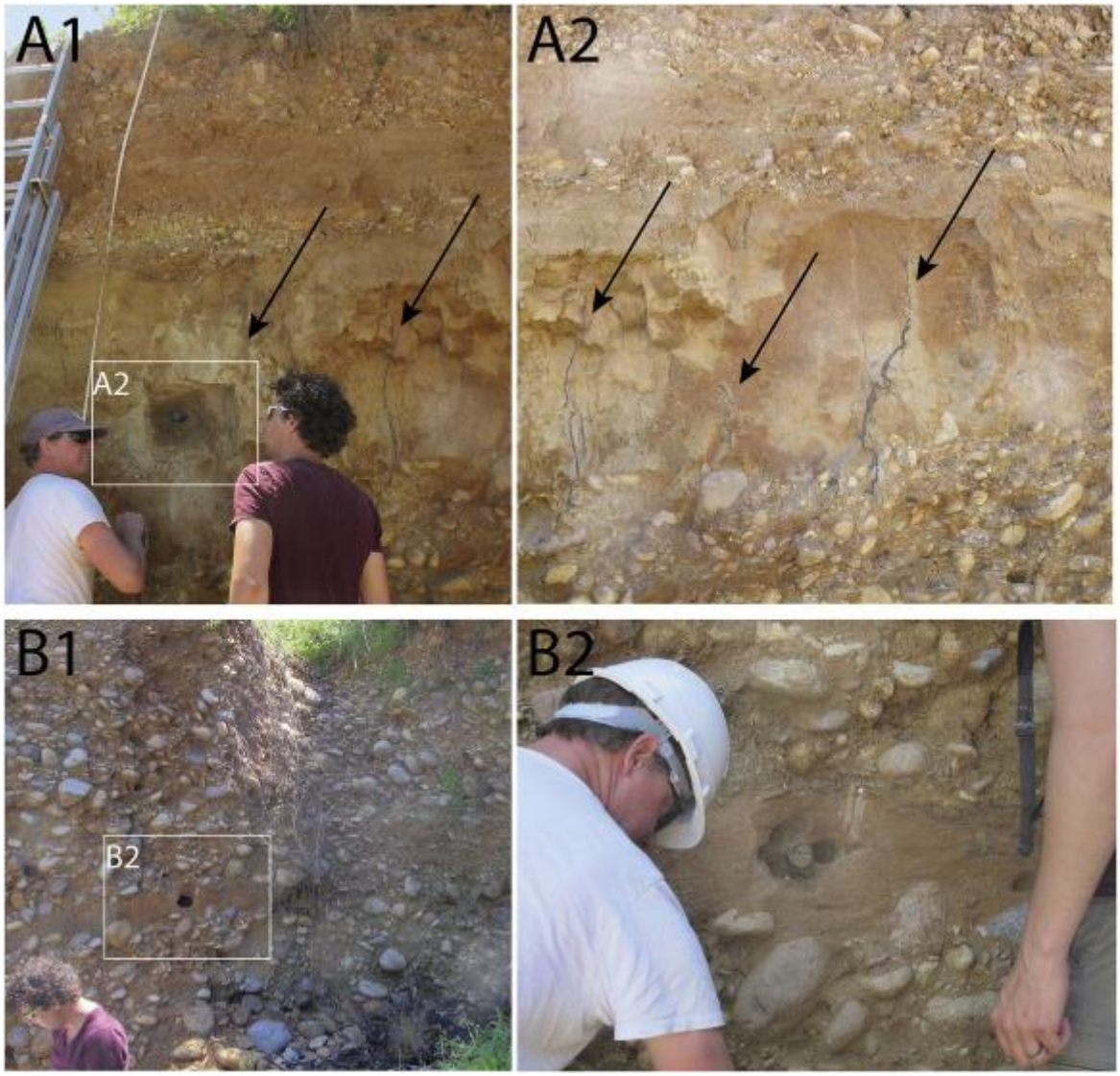

Figure 10

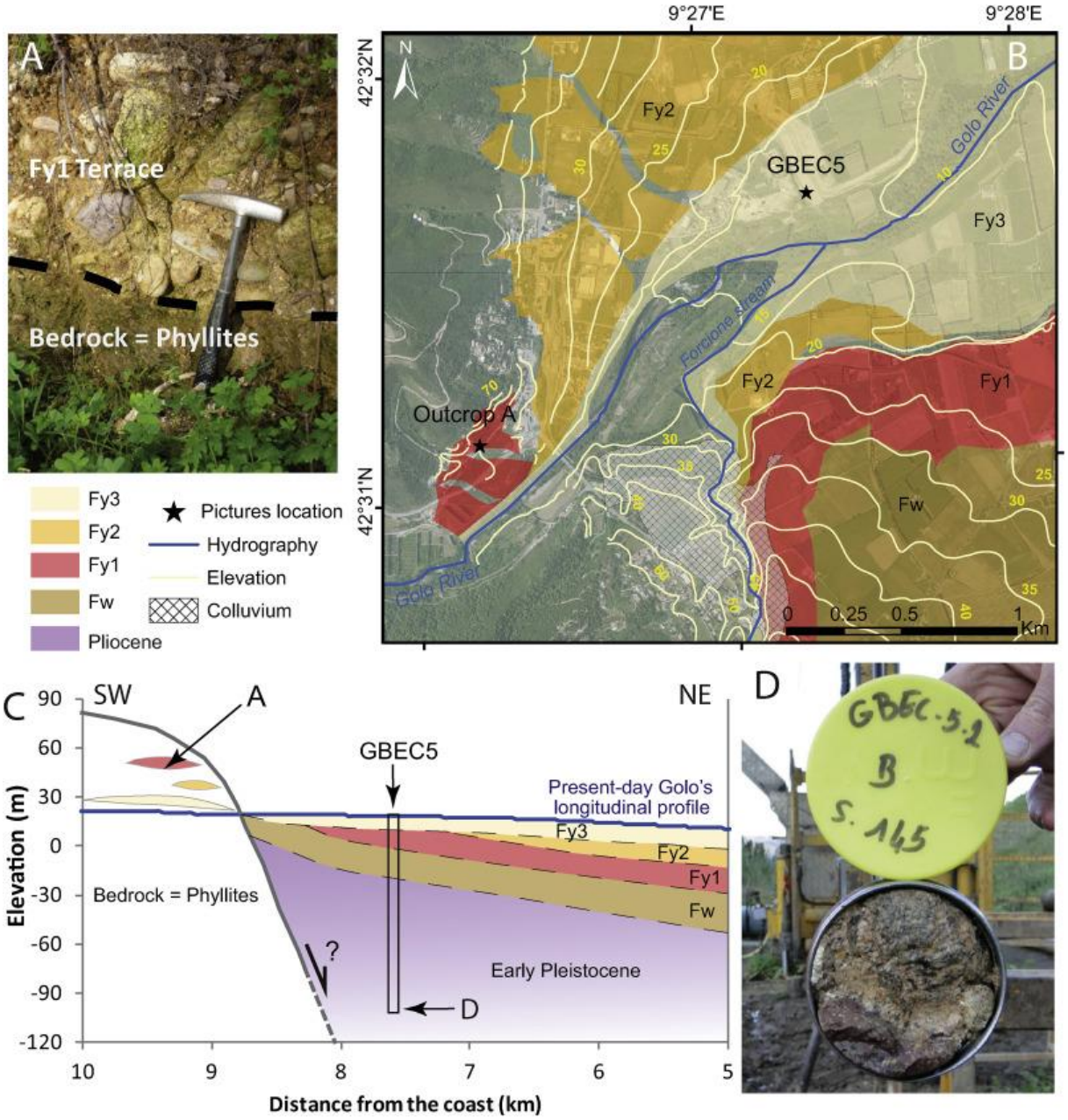
A
Fy1 Terrace
Bedrock = Phyllites
B
9°27'E
9°28'E
42°32'N
42°31'N
N
Fy2
GBEC5
Golo River
Fy3
Forcione stream
Fy2
Fy1
Outcrop A
Fw
Golo River
0 0.25 0.5 1 Km
Fy3
Fy2
Fy1
Fw
Pliocene
Pictures location
Hydrography
Elevation
Colluvium
C
SW
A
NE
GBEC5
Present-day Golo's longitudinal profile
Fy3
Fy2
Fy1
Fw
Bedrock = Phyllites
Early Pleistocene
D
Elevation (m)
Distance from the coast (km)
D
GBEC-5.2
B
S. 14,5